JCI insight

Lipidomics unveils lipid dyshomeostasis and low circulating plasmalogens as biomarkers in a monogenic mitochondrial disorder

Matthieu Ruiz, … , Yan Burelle, Christine Des Rosiers

JCI Insight. 2019;4(14):e123231. https://doi.org/10.1172/jci.insight.123231.

Research Article **Cell biology** **Metabolism**

Mitochondrial dysfunction characterizes many rare and common age-associated diseases. The biochemical consequences, underlying clinical manifestations, and potential therapeutic targets, remain to be better understood. We tested the hypothesis that lipid dyshomeostasis in mitochondrial disorders goes beyond mitochondrial fatty acid β-oxidation, particularly in liver. This was achieved using comprehensive untargeted and targeted lipidomics in a case-control cohort of patients with Leigh syndrome French-Canadian variant (LSFC), a mitochondrial disease caused by mutations in *LRPPRC*, and in mice harboring liver-specific inactivation of *Lrpprc* (H-*Lrpprc*$^{-/-}$). We discovered a plasma lipid signature discriminating LSFC patients from controls encompassing lower levels of plasmalogens and conjugated bile acids, which suggest perturbations in peroxisomal lipid metabolism. This premise was reinforced in H-*Lrpprc*$^{-/-}$ mice, which compared with littermates recapitulated a similar, albeit stronger peroxisomal metabolic signature in plasma and liver including elevated levels of very-long-chain acylcarnitines. These mice also presented higher transcript levels for hepatic markers of peroxisome proliferation in addition to lipid remodeling reminiscent of nonalcoholic fatty liver diseases. Our study underscores the value of lipidomics to unveil unexpected mechanisms underlying lipid dyshomeostasis ensuing from mitochondrial dysfunction herein implying peroxisomes and liver, which likely contribute to the pathophysiology of LSFC, but also other rare and common mitochondrial diseases.

Find the latest version:

https://jci.me/123231/pdf

JCI insight

RESEARCH ARTICLE

Lipidomics unveils lipid dyshomeostasis and low circulating plasmalogens as biomarkers in a monogenic mitochondrial disorder

Matthieu Ruiz,[1,2,3] Alexanne Cuillerier,[4] Caroline Daneault,[3] Sonia Deschênes,[3] Isabelle Robillard Frayne,[3] Bertrand Bouchard,[3] Anik Forest,[3] Julie Thompson Legault,[3] The LSFC Consortium,[5] Frederic M. Vaz,[6] John D. Rioux,[2,3] Yan Burelle,[4] and Christine Des Rosiers[1,3]

[1]Department of Nutrition and [2]Department of Medicine, Université de Montréal, Montreal, Quebec, Canada. [3]Montreal Heart Institute Research Center, Montreal, Quebec, Canada. [4]Interdisciplinary School of Health Sciences, Faculty of Health Sciences and Department of Cellular and Molecular Medicine, Faculty of Medicine, University of Ottawa, Ottawa, Ontario, Canada. [5]The list of the LSFC Consortium members is provided in Supplemental Information. [6]Amsterdam UMC, University of Amsterdam, Laboratory Genetic Metabolic Diseases, Core Facility Metabolomics, Amsterdam Gastroenterology & Metabolism, Meibergdreef, Amsterdam, Netherlands.

Mitochondrial dysfunction characterizes many rare and common age-associated diseases. The biochemical consequences, underlying clinical manifestations, and potential therapeutic targets, remain to be better understood. We tested the hypothesis that lipid dyshomeostasis in mitochondrial disorders goes beyond mitochondrial fatty acid β-oxidation, particularly in liver. This was achieved using comprehensive untargeted and targeted lipidomics in a case-control cohort of patients with Leigh syndrome French-Canadian variant (LSFC), a mitochondrial disease caused by mutations in *LRPPRC*, and in mice harboring liver-specific inactivation of *Lrpprc* (H-*Lrpprc*$^{-/-}$). We discovered a plasma lipid signature discriminating LSFC patients from controls encompassing lower levels of plasmalogens and conjugated bile acids, which suggest perturbations in peroxisomal lipid metabolism. This premise was reinforced in H-*Lrpprc*$^{-/-}$ mice, which compared with littermates recapitulated a similar, albeit stronger peroxisomal metabolic signature in plasma and liver including elevated levels of very-long-chain acylcarnitines. These mice also presented higher transcript levels for hepatic markers of peroxisome proliferation in addition to lipid remodeling reminiscent of nonalcoholic fatty liver diseases. Our study underscores the value of lipidomics to unveil unexpected mechanisms underlying lipid dyshomeostasis ensuing from mitochondrial dysfunction herein implying peroxisomes and liver, which likely contribute to the pathophysiology of LSFC, but also other rare and common mitochondrial diseases.

Introduction

Mitochondrial dysfunction is an increasingly recognized hallmark of rare and common age-related diseases. Inherited mitochondrial diseases, which have a prevalence of 1:5,000, are associated with a wide spectrum of clinical manifestations and a high mortality rate, mostly in childhood (1, 2). They predominantly affect the oxidative phosphorylation (OXPHOS) machinery (1, 2) and originate from mutations in the mitochondrial genome, or in nuclear genes encoding mitochondria-targeted proteins (2). Among the latter is the leucine-rich pentatricopeptide repeat–containing protein (LRPPRC; OMIM*607544), shown to be predominantly localized in mitochondria (3, 4).

Mutations in the *LRPPRC* gene have been identified as the root cause of a distinct monogenic form of Leigh syndrome in the French-Canadian population of the northeastern region of Quebec (Leigh syndrome French-Canadian variant; LSFC; OMIM#220111; ~1 in 2,000 births; carrier rate 1 out of 23) (5), and recently in unrelated families in Europe and China (6, 7). LSFC patients exhibit many hallmarks of inherited mitochondrial diseases such as Leigh syndrome and necrotizing encephalopathy, as well as the high occurrence of metabolic and neurological crisis, which is the main cause of mortality in young children (8, 9). LSFC

Conflict of interest: The authors have declared that no conflict of interest exists.

Copyright: © 2019, American Society for Clinical Investigation.

Submitted: June 29, 2018
Accepted: May 31, 2019
Published: July 25, 2019.

Reference information: *JCI Insight*. 2019;4(14):e123231. https://doi.org/10.1172/jci.insight.123231.

patients also show reduced tissue levels of LRPPRC as well as a decrease in mitochondria-DNA-encoded mRNAs (10, 11). This leads to an impaired tissue-specific assembly of OXPHOS complexes, principally complex IV in brain and liver, and to a lesser extent in fibroblasts and skeletal muscle (10, 11).

Impaired OXPHOS represents a major pathogenic mechanism in many mitochondrial diseases, including LSFC. However, a better understanding of the resulting perturbations in energy nutrient metabolism, which may underlie some clinical manifestations, is essential for the optimal management of patients and the design of potential interventions, which have thus far not been clearly established. LSFC patients display some lipid-handling abnormalities as evidenced from high circulating levels of long-chain acylcarnitines (LCACs), which are proxies of mitochondrial fatty acid (FA) β-oxidation perturbations (12). These patients are also affected by hepatic microvesicular steatosis (8, 13–15). Hepatic steatosis has also been reported in mice harboring liver-specific inactivation of *Lrpprc* (H-*Lrpprc*$^{-/-}$) (15) and is rescued by overexpression of *Lrpprc* in mouse liver (13, 14, 16). Of broader relevance, mitochondrial dysfunction is considered an important actor in hepatic steatosis, as it occurs in nonalcoholic fatty liver disease (NAFLD) and also more common chronic diseases (17).

Although the aforementioned perturbations in lipid metabolism are most commonly ascribed to mitochondria, the peroxisome is another often neglected organelle also playing a crucial role in the metabolism of unique classes of lipids with essential biological roles. Highly present in liver, peroxisomes are responsible for (i) the oxidation of very-long-chain (VLC) as well as branched and/or odd-numbered carbon chain FAs (18, 19), which unlike their mitochondrial counterpart are not linked to ATP formation but generate reactive oxygen species; (ii) the conjugation of primary bile acids (BAs); (iii) de novo synthesis of plasmalogens; and (iv) the terminal step of docosahexaenoic acid (DHA) biosynthesis (19). Major perturbations in these metabolic pathways have been documented in inherited peroxisomal disorders (20, 21). In addition, alterations in peroxisomal β-oxidation have been reported in animal models of hepatic steatosis (22), the latter also being a clinical manifestation in both inherited peroxisomal (18) and mitochondrial (17) disorders. Except for their contribution to LCFA oxidation (23), whether the metabolic function of peroxisomes is globally perturbed in inherited mitochondrial disorders remains, however, to be ascertained.

The objectives of this study were to test the hypothesis that lipid dyshomeostasis in mitochondrial disorders goes beyond impaired mitochondrial FA β-oxidation, and may involve, among other disturbances, changes in peroxisomal lipid metabolism. To achieve our goals, we used both untargeted and targeted lipidomics based on liquid chromatography–mass spectrometry (LC-MS) (15, 24, 25). These analyses were conducted first in our homogeneous cohort of genetically defined LSFC patients and their prospectively matched healthy controls (12). Then, we used *H-Lrpprc*$^{-/-}$ mice to evaluate the specific role of the liver (15). Our study identifies major lipid dyshomeostasis in LSFC patients and its related murine model, especially lower circulating plasmalogens as potentially novel biomarkers of LRPPRC-induced mitochondrial dysfunction. In addition, our lipidomic results are consistent with changes in peroxisomal metabolism as well as a role of the liver.

Results

Untargeted lipidomic analyses in LSFC patients versus matched healthy controls unveil major plasma lipid dyshomeostasis including lower plasmalogens. In a previous study, we used targeted metabolic profiling of energy-related metabolites in plasma samples from fasted individuals from our prospective case-control cohort and uncovered a robust signature of disrupted mitochondrial β-oxidation in LSFC patients through the accumulation of LCACs (12). The coverage of lipid metabolites beyond mitochondrial β-oxidation was, however, limited. Thus, in the present study, we applied an untargeted lipidomic workflow using high-resolution LC-quadrupole time-of-flight (LC-QTOF), which has been previously validated and shown to detect more than 1,000 reproducible MS signals or features (defined by a mass-to-charge ratio [*m/z*], retention time, and signal intensity) in human plasma samples and cover 16 lipid subclasses (25).

We analyzed plasma samples collected in the same case-control cohort under fasting conditions and after a nutrient-intake challenge. Figure 1A shows a volcano plot of all 2,052 MS features of the data set, obtained under the fasted state. Using a subjective corrected *P*-value threshold of 0.2 (corresponding to an uncorrected *P* value of 0.0034) and a fold-change (FC) >1.35 or <0.74, 29 features discriminated LSFC patients from controls, of which 14 lipids were subsequently identified by MS/MS (Supplemental Table 1; supplemental material available online with this article; https://doi.org/10.1172/jci.insight.123231DS1). The following lipid (sub)classes showed statistically significant changes (Figure 1B) — (i) increased: 2

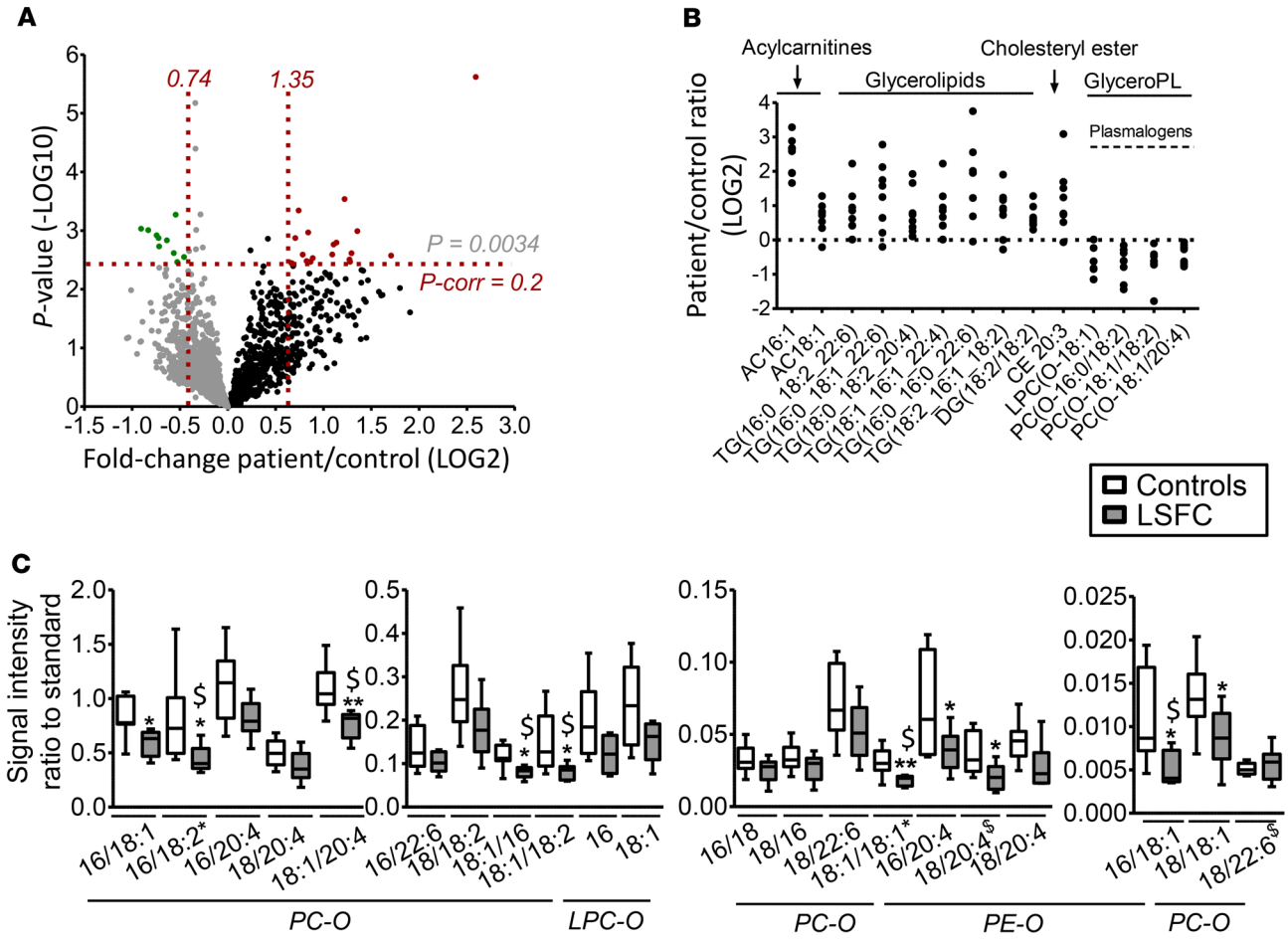

Figure 1. Untargeted and targeted lipidomics unveil major plasma lipid dyshomeostasis, including lower circulating plasmalogen levels in LSFC patients. (**A**) Volcano plot from LC-QTOF–based untargeted lipidomics of plasma from fasted LSFC and control subjects (n = 9/group) depicting the 2,052 features obtained following MS data processing. The x axis corresponds to fold changes (FCs) of MS signal intensity values for all these features in LSFC patients vs. control (log2) and the y axis to P values (–log10). Using a corrected P value (*P-corr*) threshold of 0.2 (corresponding to an uncorrected P value of 0.0034; horizontal red dotted line) and an FC >1.35 or <0.74 (vertical red dotted lines), 29 features significantly discriminated LSFC patients from controls, of which 19 were increased (red dots) and 10 decreased (green dots). See also Supplemental Table 1 for the list of lipids identified by MS/MS with FCs and P values (unpaired Student's t test followed by Benjamini-Hochberg correction). (**B**) Dot plot of 13 selected lipids significantly discriminating LSFC patients from controls and identified by MS/MS using LC-QTOF. Each dot represents a log2-transformed patient/matched control signal intensity ratio (n = 9) for the indicated lipid (sub) classes with their acyl side chain(s) — (i) 2 acylcarnitines (ACs): AC16:1 and AC18:1, (ii) 7 glycerolipids: triacylglycerol (TG) and diacylglycerol (DG), (iii) 1 cholesteryl ester (CE), (iv) 4 plasmalogens: lysophosphatidylcholine (LPC) plasmalogens (LPC-*O*) and phosphatidylcholine plasmalogens (PC-*O*). The underscore symbol "_" beside the acyl side chain for TGs refers to acyl chains for which the *sn* position remains to be ascertained. (**C**) Box plots of LC-QQQ–based lipidomic analysis of plasmalogens, 21 of which were detected in plasma from LSFC patients (gray; n = 9) and controls (white; n = 9): 2 LPC-*O*, 15 PC-*O*, and 4 phosphatidylethanolamine (PE) plasmalogens (PE-*O*). Statistics using paired Student's t test: $^{*}P < 0.05$, $^{**}P < 0.01$ before and $^{\$}$*P-corr* < 0.05 after Benjamini-Hochberg correction. See also Supplemental Figure 1, A–C, for corresponding plots of results obtained in the nutrient-uptake challenge condition.

LCACs (1.6- and 6-fold, respectively), 7 glycerolipids (1.8- to 3.3-fold), and 1 cholesteryl ester (1.7-fold); (ii) decreased: 4 phosphatidylcholine-plasmalogens (PC-plasmalogens; ~0.6-fold). It is noteworthy that all ether lipids are referred to as "plasmalogens," although MS/MS could not always distinguish plasmanyl (O-alkyl) from plasmenyl (P-alkyl) glycerophospholipids. Similar results were obtained using samples collected after the nutrient-intake challenge (Supplemental Figure 1, A and B).

Targeted lipidomics in LSFC patients ascertains the presence of perturbations in peroxisomal lipid and FA metabolism secondary to their mitochondrial dysfunction. Among all aforementioned lipids discriminating LSFC patients from controls, we focused on plasmalogens given that they are recognized hallmarks of primary peroxisomal defects (i.e., Zellweger and rhizomelic chondroplasia punctata syndromes; refs. 25, 26). To further support our hypothesis of a contribution of peroxisomes to lipid dyshomeostasis in LSFC patients, additional targeted analyses were performed using LC–triple quadrupole (LC-QQQ). First, we expanded the coverage of plasmalogens. Second, we sought to assess changes in other lipid species relevant to peroxisomal metabolism, namely (i) FA species

with a very-long-chain (VLCFAs; >20 C), which cannot be oxidized by mitochondria, or with an odd chain, generated from dietary phytanic acid metabolism (18), and (ii) C24 BAs conjugated with glycine (glyco-BA) or taurine (tauro-BA) (19, 26). In parallel, plasma samples were also analyzed by a certified laboratory for established biomarkers in inherited peroxisomal disorders, specifically C26:0-lysophosphatidylcholine (LPC 26:0) (27, 28) and the BA intermediates di- and trihydroxycholestanoic (DHCA and THCA) (29).

First, analyses of plasmalogens using LC-QQQ not only confirmed, but also expanded those using untargeted lipidomics; out of the 21 PC- and phosphatidylethanolamine-plasmalogens (PE-plasmalogens) detected in plasma, 10 (3 of which were identified in the untargeted analysis) showed significantly lower levels in LSFC patients versus controls (between 0.5- and 0.7-fold) in the fasted state (Figure 1C) as well as following the nutrient-intake challenge (Supplemental Figure 1C), of which 6 remained significant after Benjamini-Hochberg correction.

Second, we conducted the profiling of 91 ACs, which are considered circulating proxies of alterations in cellular FA metabolism in mitochondria and beyond (24). In both conditions tested, nearly 25% of all measured ACs were increased (1.5- to 5-fold) in LSFC patients (significance threshold $P < 0.05$) after nutrient challenge (Figure 2A) and fasting (Supplemental Figure 2A). These included, among the most discriminant (corrected $P < 0.05$), various AC species with saturated and unsaturated, hydroxylated even-numbered carbon chains, which reflect perturbations in mitochondrial LCFA β-oxidation (Figure 2B and Supplemental Figure 2B). As for proxies of peroxisomal metabolism, changes encompassed odd-numbered carbon chain ACs (Figure 2B and Supplemental Figure 2B), albeit VLCAC (>20 C) did not reach significance after Benjamini-Hochberg correction. Quantitative analyses for established biomarkers in inherited peroxisomal diseases, AC26:0 and LPC 26:0, revealed also no significance changes between LFSC patients and controls (Figure 2C and Supplemental Figure 2C).

Regarding plasma BA species, while LSFC patients had levels of unconjugated BAs similar to control subjects under both conditions tested (Figure 2D and Supplemental Figure 2D), those of glyco-BAs — glycochenodeoxycholic acid (GCDCA), glycocholic acid (GCA), glycodeoxycholic acid (GDCA), and taurocholic acid (TCA) (Figure 2E) — were all reduced by approximately 50% ($P < 0.05$), albeit only in the fasting condition (Figure 2, E and F, and Supplemental Figure 2, E and F). Lastly, levels of THCA and DHCA were undetectable under all conditions (data not shown).

Collectively, our findings of lower plasma levels of plasmalogens and conjugated BAs in LSFC patients support a contribution of peroxisomes to lipid dyshomeostasis in these patients. This contribution appears, however, more subtle than that reported in primary peroxisomal disorders, as suggested by the absence of changes in their established biomarkers. Hence, to better understand the plasma lipid dyshomeostasis observed in LSFC patients and the role of peroxisomes, we extended our lipidomic investigation to the H-*Lrpprc*$^{-/-}$ mouse.

Lipidomics and molecular analyses in the H-Lrpprc$^{-/-}$ *mouse corroborate the plasma lipid dyshomeostasis of LSFC patients, including lower plasmalogens, and unveil a role of the liver*. The H-*Lrpprc*$^{-/-}$ mouse model, which harbors a liver-specific loss of function of *Lrpprc,* was previously investigated and shown to display at 5 weeks major mitochondrial bioenergetic defects in the liver, which are characteristic of LSFC patients (>90% and 80% lower protein levels for LRPPRC and COX subunit COX1, respectively), and to recapitulate histopathological changes characteristic of microvesicular steatohepatitis (15, 16). In the present study, we used H-*Lrpprc*$^{-/-}$ mice that had reached 14 weeks of age, and confirmed lower protein levels in liver for LRPPRC and COX subunit MTCO1 (60% and 30%, respectively; Supplemental Figure 3), although the observed changes were less pronounced than at 5 weeks. This difference can likely be ascribed to the occurrence of liver regeneration with age in albumin-CRE mouse models (30). Nevertheless, as shown below, at 14 weeks, H-*Lrpprc*$^{-/-}$ mice display major metabolic alterations both in plasma and liver compared with their littermate counterparts.

Lipidomics in plasma samples. In these same mice, we performed untargeted lipidomics of plasma samples and resolved 1,295 MS features (Figure 3A). Using a subjective corrected *P*-value threshold of 0.05 (corresponding to an uncorrected *P* value of 0.01) and an FC >2 or <0.5, a total of 98 features discriminated H-*Lrpprc*$^{-/-}$ mice from controls, of which 35 unique compounds were identified by MS/MS (Supplemental Table 2). The observed changes were similar to LSFC patients and encompassed the following lipid (sub)classes — (i) increased: glycerolipids (11 species; Figure 3B) and AC (1 LCAC with 18 carbons; Figure 3B); and (ii) decreased: glycerolipids (4 species; Figure 3B) and PE-plasmalogens (2 species; Figure 3D), the latter findings being consistent with a peroxisomal metabolic signature. Our finding of decreased plasmalogens in plasma of H-*Lrpprc*$^{-/-}$ mice was further ascertained by manually aligning our mouse data

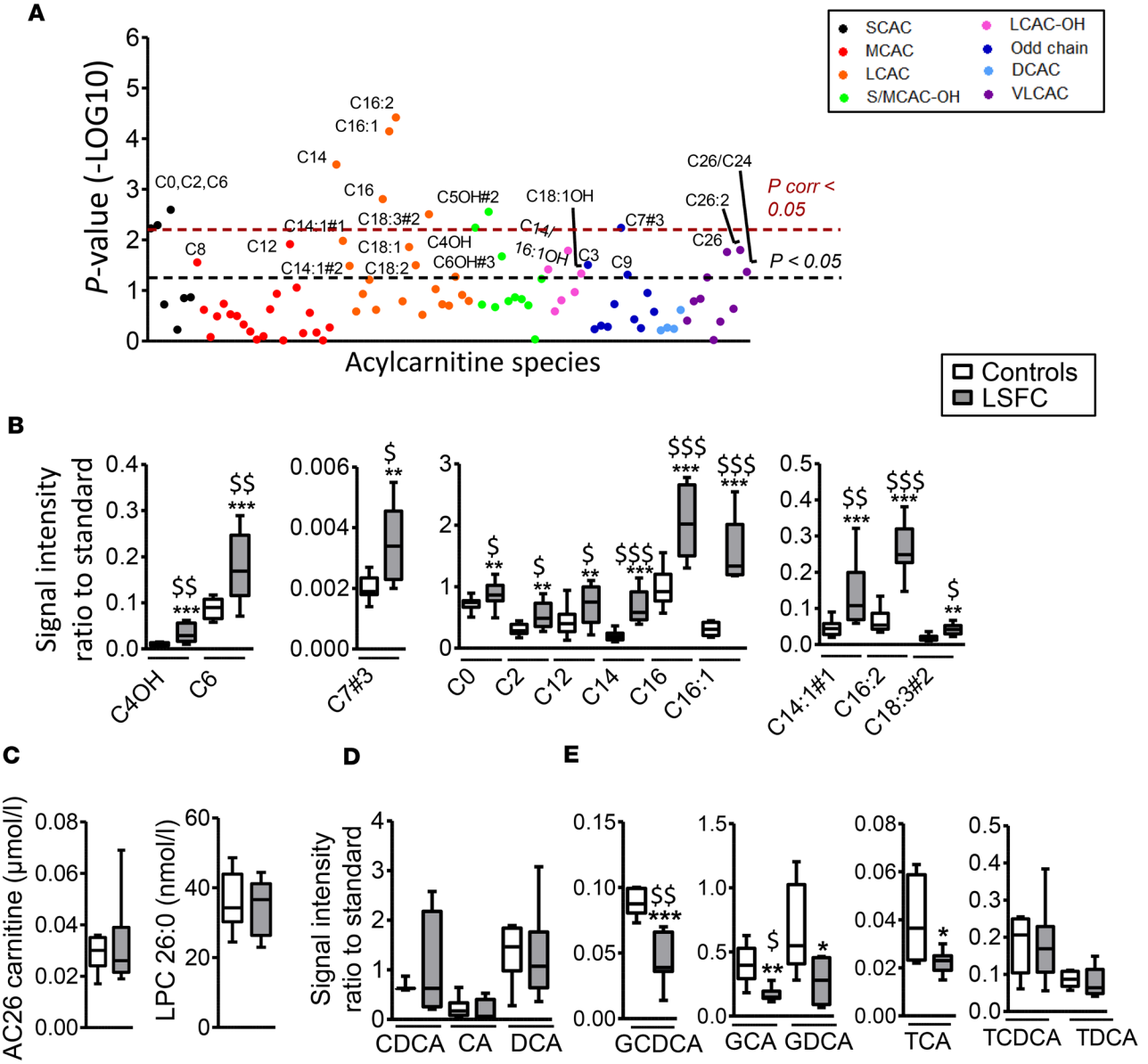

Figure 2. Targeted profiling of acylcarnitines (ACs) and lysophosphatidylcholine (LPC) 26:0 and unconjugated/conjugated bile acids (BAs) reveals additional lipid perturbations in plasma from LSFC patients. (**A** and **B**) LC-QQQ–based profiling of 91 ACs in plasma from LSFC patients (gray; $n = 9$) and controls (white; $n = 9$) after a nutrient-uptake challenge. (**A**) Dot plot of P values obtained using paired Student's t test analysis for the various AC species: short-chain (SCAC, black), medium-chain (MCAC, red), long-chain (LCAC, orange), hydroxylated short/medium–chain (S/MCAC-OH, green), hydroxylated long-chain (LCAC-OH, pink), odd-numbered carbon chain (dark blue), dicarboxylic (DCAC, light blue), and very-long-chain (VLCAC, purple). Significantly elevated ACs are above the dotted line (black $P < 0.05$, red $P\text{-}corr < 0.05$). (**B**) Box plots of selected significantly (according to $P\text{-}corr$) elevated AC species in LSFC patients (gray) and controls (white). Cx refers to the number of carbons in the acyl chain of AC species and the symbol # to isomers of AC species, of which the structure remains to be ascertained (e.g., AC#1, AC#2, etc.). (**C**) Box plots of quantitative values for VLCAC (AC26:0) and LPC 26:0. (**D** and **E**) Box plots from LC-QQQ–based profiling of plasma from fasted LSFC patients (gray; $n = 4$–9) and controls (white; $n = 6$–9) for (**D**) unconjugated BA, (**E**) glyco- and tauro-conjugated BAs. Unequal distribution is ascribed to values below the limit of detection. Statistics using 2-tailed unpaired Student's t test: $^{*}P < 0.05$, $^{**}P < 0.01$, $^{***}P < 0.001$ before and $^{\$}P < 0.05$, $^{\$\$}P < 0.01$, $^{\$\$\$}P < 0.001$ after Benjamini-Hochberg correction. CA, cholic acid; CDCA, chenodeoxycholic acid; DCA, deoxycholic acid; GCA, glycocholic acid; GDCA, glycodeoxycholic acid; GCDCA, glycochenodeoxycholic acid; TCA, taurocholic acid; TDCA, taurodeoxycholic acid; TCDCA, taurochenodeoxycholic acid. See also Supplemental Figure 2, A–C, for corresponding plots of results obtained for the fasting and Supplemental Figure 2, D–F, for nutrient-uptake challenge condition.

set with previously acquired human and mouse reference data sets for which the various plasmalogens had been previously identified by MS/MS. This approach allowed the identification of 12 additional PE- and PC-plasmalogens; 11 were significantly decreased in H-*Lrpprc*$^{-/-}$ samples, of which 3 remained significantly lower after Benjamini-Hochberg correction (~0.6-fold; Figure 3E).

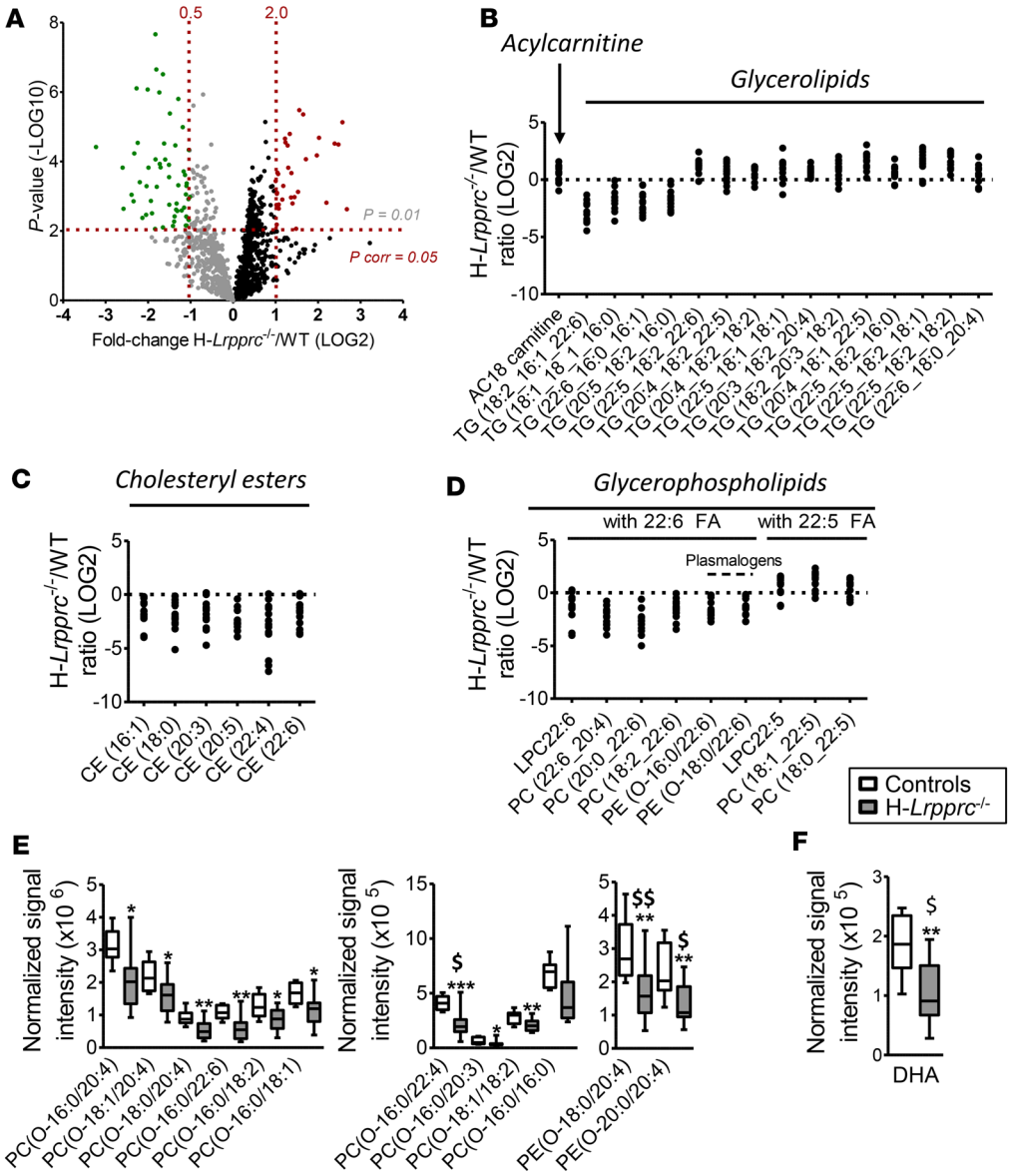

Figure 3. Untargeted lipidomics in plasma from H-*Lrpprc*$^{-/-}$ mice identifies multiple lipid changes including lower levels of plasmalogens and docosahexaenoic acid (DHA). (**A**) Volcano plot of LC-QTOF–based untargeted lipidomics from plasma of fed H-*Lrpprc*$^{-/-}$ mice (n = 13) and their littermate controls (n = 8) depicting the 1,295 features obtained following MS data processing. Using a *P-corr* threshold of 0.05 (corresponding to an uncorrected P value of 0.01; horizontal red dotted line) and a FC >2 or <0.5 (vertical red dotted lines), 98 features significantly discriminated H-*Lrpprc*$^{-/-}$ mice vs. controls, of which 32 were increased (red dots) and 66 were decreased (green dots). See also Supplemental Table 2 for the list of lipids identified by MS/MS with FCs and P values (2-tailed unpaired Student's t test and with Benjamini-Hochberg correction). (**B**–**D**) Dot plots of selected lipids significantly discriminating H-*Lrpprc*$^{-/-}$ mice from controls and identified by MS/MS using LC-QTOF. Each dot represents a log2-transformed signal intensity ratio for the indicated lipid (sub)classes with their acyl side chain(s): (**B**) 1 AC: AC18:0 and 15 glycerolipids (TGs); (**C**) 6 CEs; (**D**) 9 glycerophospholipids: 2 LPC, 5 PC, and 2 PE-plasmalogens (PE-*O*). The underscore symbol "_" beside the acyl side chain for TGs and glycerophospholipids refers to acyl chains for which the *sn* position remains to be ascertained. (**E** and **F**) Box plots of (**E**) plasmalogens and (**F**) DHA identified through manual alignment of this mouse plasma data set with human and mouse reference data sets for which the various plasmalogens had been previously identified by MS/MS. Statistics using 2-tailed unpaired Student's t test: $^{*}P < 0.05$; $^{**}P < 0.01$, $^{***}P < 0.001$ before and $^{\$}P < 0.05$, $^{\$\$}P < 0.01$ after Benjamini-Hochberg correction.

There were also additional changes that reached statistical significance in H-*Lrpprc*$^{-/-}$ mice but that were not observed in LSFC patients. These included 13 lipid species that were (i) increased, namely 3 PCs containing 22:5 FA (Figure 3D); or (ii) decreased, namely 4 PCs containing DHA (Figure 3D); and 6 cholesteryl esters including 1 containing DHA (Figure 3C). Furthermore, consistent with these changes in lipid-containing DHA, plasma levels of free DHA were also significantly decreased (–45%, $P < 0.01$) in H-*Lrpprc*$^{-/-}$ mice versus controls (Figure 3F). These findings further support the contribution

of peroxisomes, given that the last step of DHA (22:6) synthesis occurs only in these organelles (19). Similar to LSFC patients, there were, however, no significant changes in plasma levels of VLCACs (>20 C) and LPC 26:0 (Supplemental Figure 4).

In summary, results from our untargeted lipidomic analysis demonstrate that our mouse model of liver-specific LRPPRC-dependent mitochondrial dysfunction recapitulates most of the plasma lipid perturbations observed in LSFC patients, including changes supporting a contribution of peroxisomes.

Lipidomics in liver samples. To further assess the role of liver in the lipid perturbations observed in plasma, we performed untargeted analyses of hepatic samples and resolved 1,386 MS features (Figure 4A). Using a subjective corrected *P*-value threshold of 0.05 (corresponding to an uncorrected *P* value of 0.015) and an FC >2.5 or <0.4, a total of 92 features discriminated H-*Lrpprc*$^{-/-}$ mice from controls, corresponding to 41 unique lipids (Supplemental Table 3) that encompass the following (sub)classes: (i) 15 glycerolipids (9 increased 2.8- to 5.0-fold, 6 decreased 0.16- to 0.35-fold; Figure 4B); (ii) glycerophospholipids, 9 PCs (6 increased 2.9- to 7.4-fold, 3 decreased ~0.3- to 0.4-fold; Figure 4C) and 9 PEs (increased 2.6- to 5.9-fold; Figure 4C); as well as (iii) ACs, mostly LCACs (4 increased 3- to 3.6-fold; Figure 4D), the latter being consistent with defective mitochondrial β-oxidation. Collectively, the hepatic lipid signature of H-*Lrpprc*$^{-/-}$ mice revealed by untargeted lipidomics is reminiscent of that observed in NAFLD (31, 32). Although this signature did not include any lipid species specifically reflecting peroxisomal metabolism, this does not preclude the presence of such changes since they may not have made the arbitrarily chosen strict cutoff of a corrected *P* value of 0.05 and FC >2.5 or <0.4 that was selected for discriminating the 2 mouse groups with this data set. In fact, additional analyses for plasmalogens, through manual alignment of data sets as performed above for plasma, enabled identification of 9 plasmalogens (Figure 5A) that differed significantly in H-*Lrpprc*$^{-/-}$ versus control mice, of which 7 remained significant after Benjamini-Hochberg correction.

Furthermore, targeted analyses of ACs and BAs in liver of H-*Lrpprc*$^{-/-}$ and control mice also identified significant changes (corrected $P < 0.05$, corresponding to $P < 0.035$) in these lipid (sub)classes. Specifically, changes included higher levels for 28 ACs comprising several even-carbon, hydroxylated or nonhydroxylated ACs with <20 C as well as VLCACs and odd-numbered carbon chain ACs (Figure 5B). Our finding of higher levels of VLCACs was further investigated using targeted LC-QQQ profiling of 6 VLCACs (>20 C) and 1 VL-LPC; significantly higher values were found (after Benjamini-Hochberg correction) for 3 VLCAC species including AC26:0, albeit not for LPC 26:0 (Figure 5C). As for BA species, the ratio of conjugated versus unconjugated derivatives was significantly decreased in liver from H-*Lrpprc*$^{-/-}$ mice (Figure 5D).

Collectively, the observed changes in plasmalogens, odd-numbered carbon chain and VLC-ACs, as well as in the ratio of conjugated versus unconjugated BAs in livers of H-*Lrpprc*$^{-/-}$ mice provide additional support for a contribution of peroxisomes to lipid dyshomeostasis in this study model.

Transcriptional analyses in liver samples. To provide additional insight into the metabolic changes occurring in the liver of H-*Lrpprc*$^{-/-}$ mice, we measured transcript levels of selected markers of mitochondrial and peroxisomal lipid metabolism as well as of biogenesis and transport. Concurring with previously reported mitochondrial abnormalities in this *Lrpprc*-deficient mouse model, there were significant changes in expression for some genes involved in β-oxidation (Supplemental Figure 6A), especially *CptII* and *Mcad* (up 1.6-fold, $P < 0.05$ and $P < 0.01$, respectively), whereas those for genes involved in mitochondrial biogenesis did not reach significance (Supplemental Figure 6B), namely *Pgc-1α* (up 2-fold, $P = 0.1$), *Prc* (up 1.5-fold, $P = 0.08$), *Nrf1* (up 1.4-fold, $P = 0.05$), and *Tfam* (1.2-fold, $P = 0.1$). Regarding peroxisomal gene transcripts, statistically significant changes were observed for enzymes catalyzing β-oxidation (Figure 6A) of VLCFAs (*Ehhadh*: up 1.4-fold, $P < 0.01$ and *Acox1*, down 40%; $P < 0.05$); for several markers of peroxisomal biogenesis and transport processes (Figure 6, B and C), especially *Pex11β* (1.5-fold, $P < 0.001$), *Pex14* (1.6-fold, $P < 0.01$), *Pex19* (1.4-fold, $P < 0.05$), *Pex1* (1.4-fold, $P < 0.05$), and *Pex10* (1.5-fold, $P < 0.05$); as well as for a direct marker of peroxisome content, namely catalase (up 1.3-fold, $P < 0.01$; Figure 6D). Finally, further supporting our finding in this study of changes in plasmalogens in this mouse model, there was a strong and significant increase in the gene expression for *Far1* (1.5-fold, $P < 0.01$; Figure 6E), a sensor of their intracellular levels (33, 34), as well as for *Agps* (1.7-fold, $P < 0.01$; Figure 6E), an enzyme involved in the initial steps of their biosynthesis (35).

Collectively, results from lipidomic and molecular analyses in livers of H-*Lrpprc*$^{-/-}$ mice provide further evidence for the presence of major lipid dyshomeostasis subsequent to LRPPRC-induced mitochondrial dysfunction, as well as for a contribution of peroxisomes based on the observed changes in levels of plasmalogens, conjugated BAs, and VLCACs (>20 C). These results also identify the liver as a major player.

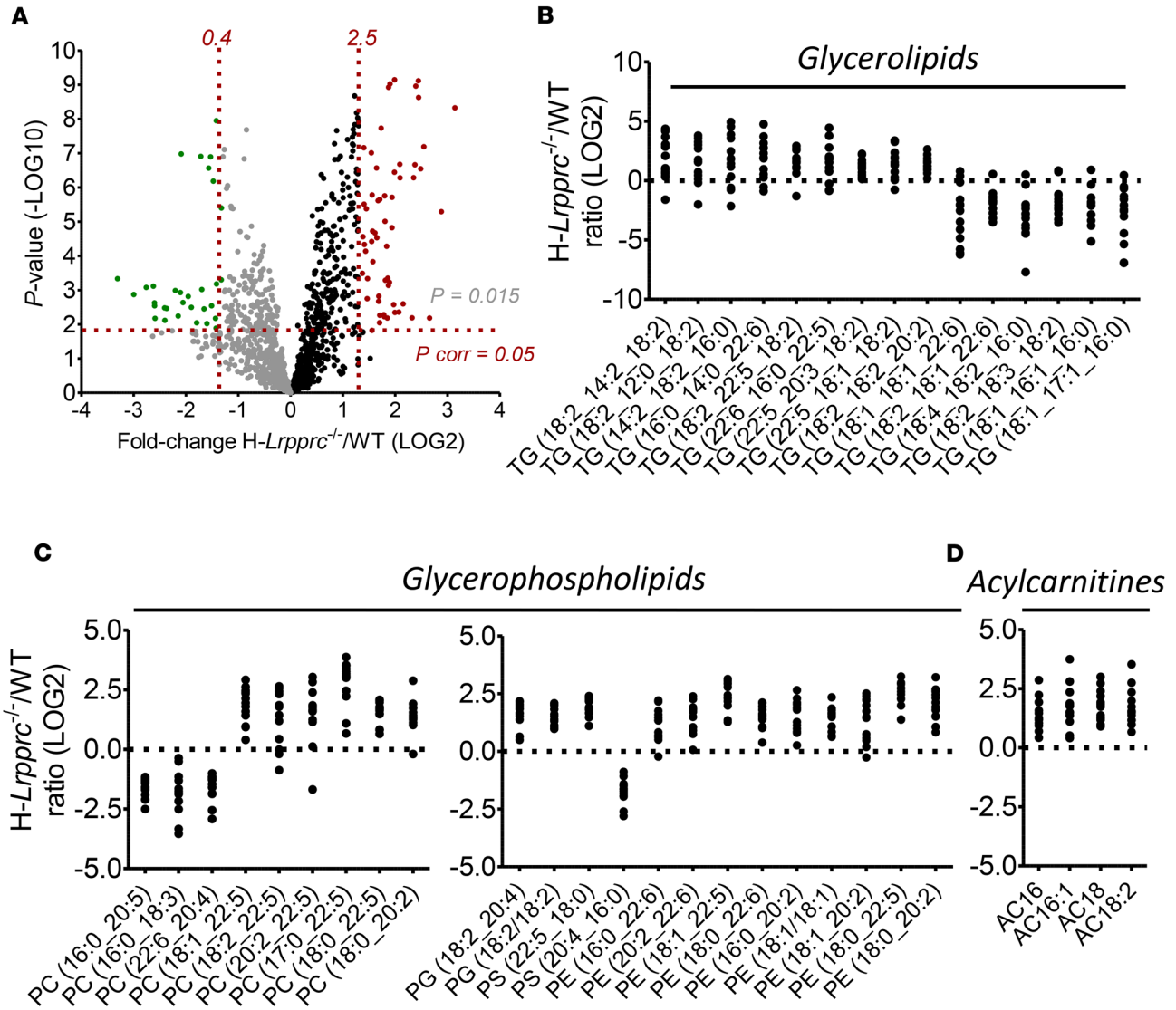

Figure 4. Untargeted lipidomics reveals major lipid perturbations in livers from H-*Lrpprc*$^{-/-}$ mice characteristic of nonalcoholic fatty liver disease. (**A**–**D**) LC-QTOF–based untargeted lipidomics from livers of fed H-*Lrpprc*$^{-/-}$ mice (n = 13) and their littermate controls (n = 8). (**A**) Volcano plot depicting the 1,386 features obtained following MS data processing. Using a *P-corr* threshold of 0.05 (corresponding to an uncorrected P value of 0.015; horizontal red dotted line) and an FC >2.5 or <0.4 (vertical red dotted lines), 92 features significantly discriminated H-*Lrpprc*$^{-/-}$ mice vs. controls, of which 60 were increased (red dots) and 32 decreased (green dots). See also Supplemental Table 3 for the list of lipids identified by MS/MS with FCs and P values (unpaired Student's t test and with Benjamini-Hochberg correction). (**B**–**D**) Dot plots of selected lipids significantly discriminating H-*Lrpprc*$^{-/-}$ mice from controls and identified by MS/MS. Each dot represents a log2-transformed signal intensity ratio for the indicated lipid (sub)classes with their acyl side chain(s): (**B**) 15 glycerolipids (TGs); (**C**) 22 glycerophospholipids: 9 PC, 9 PE, 2 phosphatidylglycerol (PG) and 2 phosphatidylserine (PS); and (**D**) 4 ACs.

Discussion

In this study, we applied an untargeted comprehensive lipidomic approach in human and mouse carrying LRPPRC-dependent mitochondrial dysfunction and unveiled a major lipid dyshomeostasis. The observed perturbations in lipid metabolism go beyond the mitochondria and suggest involvement of its close metabolic partner, the peroxisome. This is supported by our findings of changes in plasma and/or hepatic levels of plasmalogens, VLCACs, and BA conjugates, which were documented under different nutritional conditions, namely in the fasted and/or absorptive state for LSFC patients, and fed state for mice. Additional data in H-*Lrpprc*$^{-/-}$ mouse livers further substantiate these changes using molecular markers of peroxisomal remodeling, and reveal a lipidomic signature that is reminiscent of NAFLD.

Loss of LRPPRC disrupts mitochondrial FA β-oxidation. Results from this study concur with our previous findings in LSFC patients (plasma) of perturbations in FA metabolism in mitochondria (12). This is revealed by higher circulating levels of various ACs, especially saturated and unsaturated LCACs, which are recog-

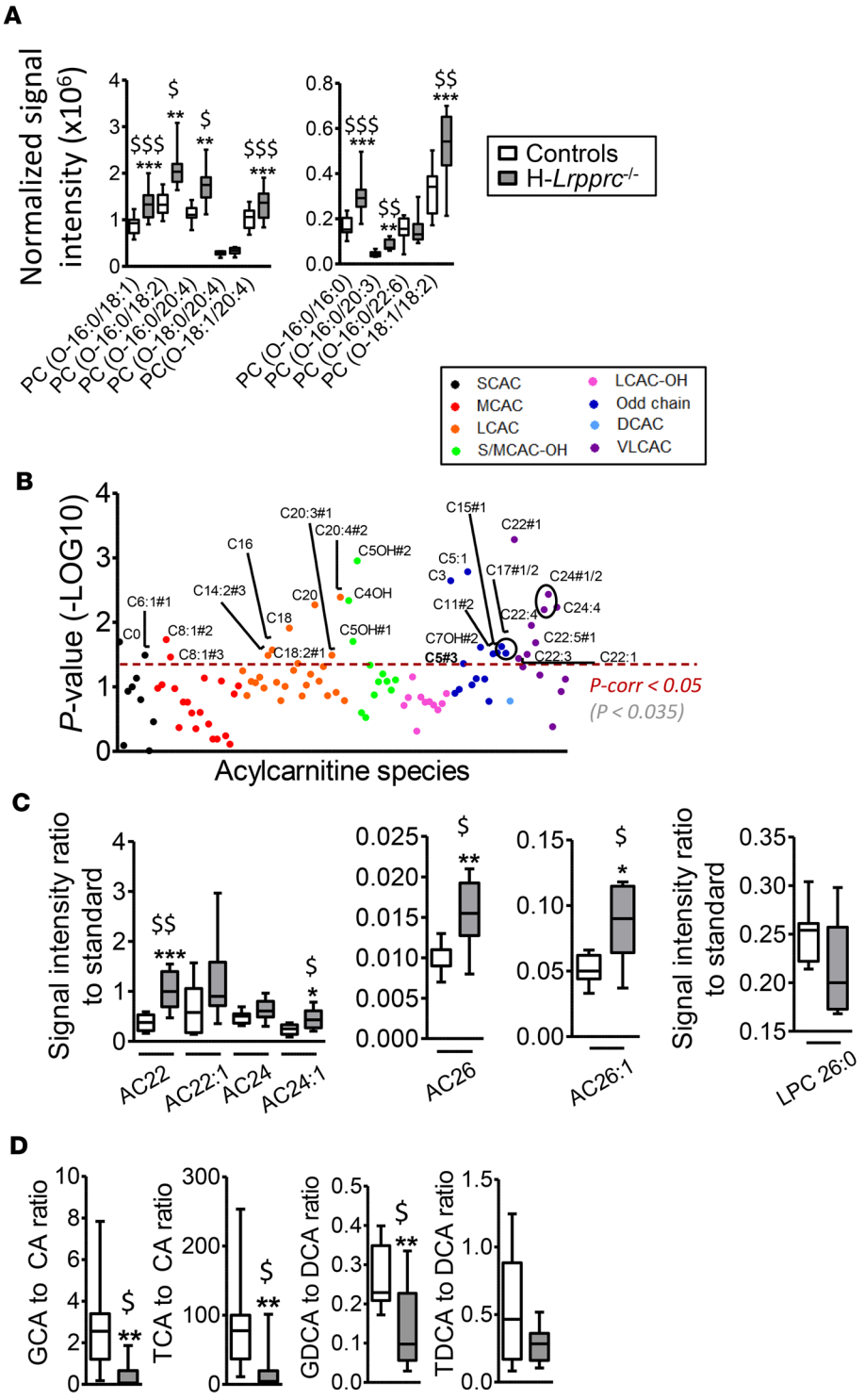

Figure 5. Hepatic levels of plasmalogens, acylcarnitines (ACs), and bile acids (BAs) in H-*Lrpprc*$^{-/-}$ mice are consistent with peroxisomal lipid metabolism remodeling. LC-MS–based analysis of livers from fed H-*Lrpprc*$^{-/-}$ mice (n = 13; gray) and their littermate controls (n = 8; white). (**A**) Box plots of 9 plasmalogens identified through manual alignment of mouse plasma data set with human and mouse reference data sets for which the various plasmalogens had been previously identified by MS/MS. (**B**) Dot plot of P values obtained using paired Student's t test analysis for the various AC species: short-chain (SCAC, black), medium-chain (MCAC, red), long-chain (LCAC, orange), hydroxylated short/medium–chain (S/MCAC-OH, green), hydroxylated long-chain (LCAC-OH, pink), odd-numbered carbon chain (dark blue), dicarboxylic (DCAC, light blue), and very-long-chain (VLCAC, purple). Significantly elevated ACs are above the dotted line (P-$corr$ < 0.05 corresponding to a P value of 0.035). See also Supplemental Figure 5 for the most representative increased ACs. (**C**) Box plots of LC-QQQ–based profiling of VLC-ACs and LPC 26:0. (**D**) Box plots of LC-QQQ–based analysis of conjugated/unconjugated BAs expressed as ratios. Statistics using 2-tailed unpaired Student's t test: $^{*}P < 0.05$; $^{**}P < 0.01$, $^{***}P < 0.001$ before and $^{\$}P < 0.05$, $^{\$\$}P < 0.01$, $^{\$\$\$}P < 0.001$ after Benjamini-Hochberg correction.

nized proxies of mitochondrial FA β-oxidation. Our results also extend these previous findings by identifying changes in the levels of hydroxylated ACs, which were also elevated. This was not only observed in plasma samples from LSFC patients (for both long- and short-chain ACs), but also in the liver of H-*Lrpprc*$^{-/-}$ mice (for short-chain ACs). The accumulation of these specific lipids points to a defect at the third step of the β-oxidation cycle (36). This step is catalyzed by 3-hydroxyacyl-CoA dehydrogenase, which is favored in the presence of NAD^+ (37). In LSFC patients, we have previously reported higher plasma β-hydroxybutyrate levels and β-hydroxybutyrate to acetoacetate ratio, a surrogate of mitochondrial NADH to NAD^+ ratio (12, 38). This suggests lower NAD^+ bioavailability, which would be unfavorable for the 3-hydroxyacyl-CoA-dehydrogenase

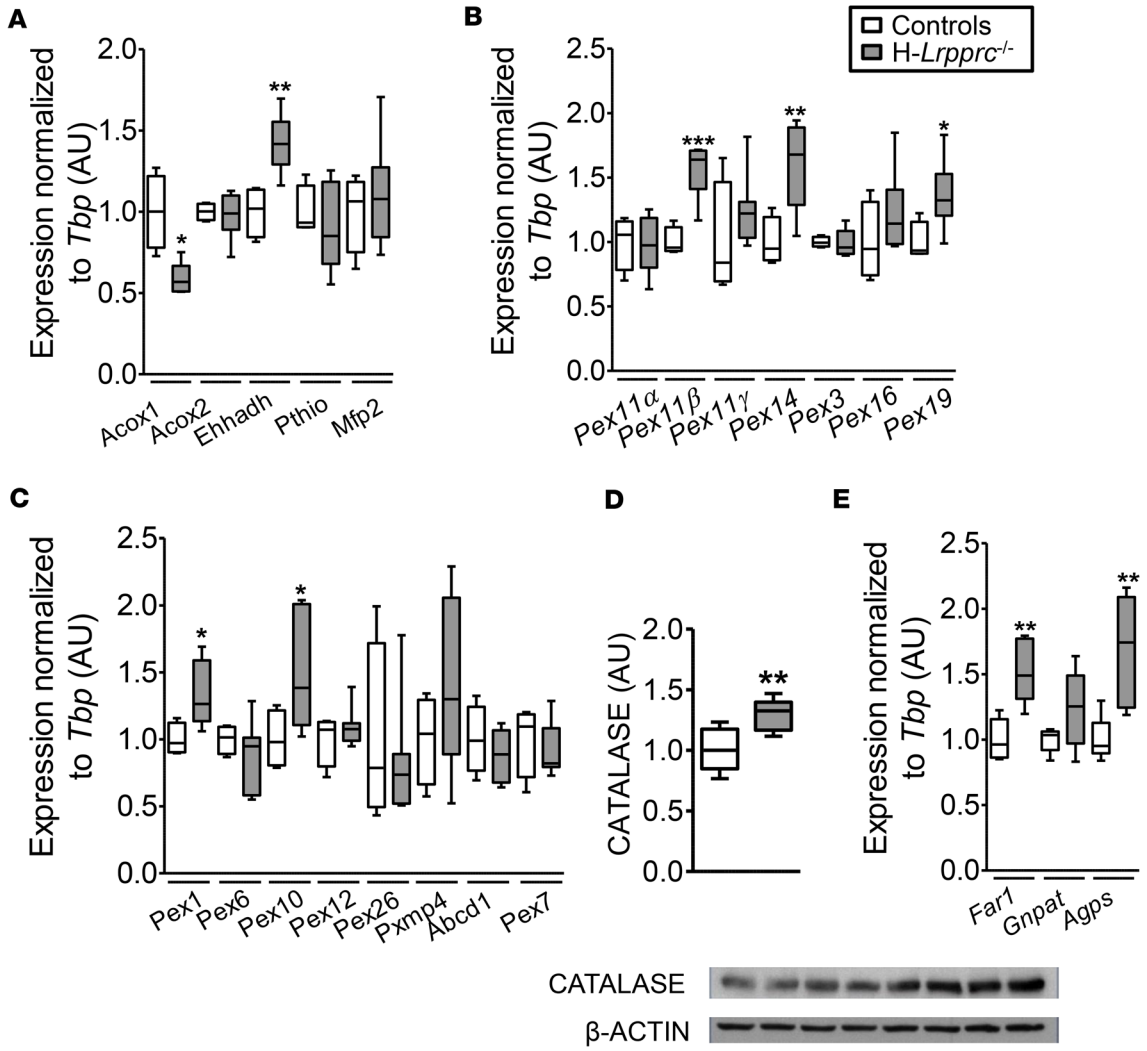

Figure 6. Livers from H-*Lrpprc*$^{-/-}$ mice display changes in molecular markers of biogenesis, fatty acid oxidation, and plasmalogen synthesis in peroxisomes. Levels of transcripts and protein were assessed in whole-liver extracts from H-*Lrpprc*$^{-/-}$ mice (gray, $n = 13$) and controls (white, $n = 8$). (**A**–**D**) Box plots depicting levels of mRNA, normalized to *Tbp*, are shown for markers of (**A**) fatty acid oxidation (*Acox1*, *Acox2*, *Ehhadh*, *Pthio*, *Mfp2*), (**B**) peroxisomal biogenesis (*Pex11α*, *Pex11β*, *Pex11γ*, *Pex14*, *Pex3*, *Pex16*, *Pex19*), and (**C**) transport (*Pex1*, *Pex6*, *Pex10*, *Pex12*, *Pex26*, *PXMP4*, *ABCD1*, *Pex7*). (**D**) Representative image and quantitation (histogram) of catalase and β-actin protein expression. (**E**) Markers of plasmalogen synthesis (*Far1*, *Gnpat*, *Agps*). *$P < 0.05$, ** $P < 0.01$, ***$P < 0.001$ using 2-tailed unpaired Student's *t* test.

activity. The importance of the liver in eliciting the observed plasma metabolite changes, including hydroxylated ACs, is supported by our findings in H-*Lrpprc*$^{-/-}$ mice, and previous studies documenting impaired LCFA oxidation in liver mitochondria (14–16). Conversely, overexpression of *Lrpprc* in mouse liver improved LCFA oxidation and was accompanied by increased hepatic OXPHOS and tissue NAD^+ levels (16).

LRPPRC-dependent mitochondrial dysfunction is associated with changes in peroxisomal lipids, especially plasmalogens. Beyond the aforementioned changes in levels of various ACs ascribed to an altered mitochondrial FA β-oxidation in LSFC patients and H-*Lrpprc*$^{-/-}$ mice, our lipidomic results also identify other major lipid perturbations that go beyond mitochondria. A remodeling of peroxisomal lipid metabolism is supported by our combined findings in LSFC patients and (plasma) and H-*Lrpprc*$^{-/-}$ mice (plasma and liver) of changes in plasmalogens, conjugated BA, VLCACs, and DHA. While many of these observed changes are reminiscent of those reported in primary peroxisomal disorders, they are, however, generally more subtle, which would be expected given that they are secondary to a primary mitochondrial dysfunction.

First, the observed changes in H-*Lrpprc*$^{-/-}$ mice, albeit not in LSFC patients, in VLCACs (AC26:0) (higher in liver), DHA (lower in plasma), and *Acox1* gene expression (lower in liver) support a defect in

peroxisomal FA β-oxidation. In addition, the levels of odd-numbered carbon chain ACs (higher in LSFC patients and H-*Lrpprc*$^{-/-}$ mice) may suggest impaired oxidation of phytanic acid (18). Such changes and oxidation defects are hallmarks of primary inherited peroxisomal disorders (i.e., X-linked adrenoleukodystrophy; ref. 39) and *ACOX1* deficiency (40). In the latter conditions, there are, however, additional major metabolic changes, which were not observed in H-*Lrpprc*$^{-/-}$ mice or in LSFC patients, which include higher circulating levels of LPC 26:0, which is considered a more sensitive marker than AC26:0 of primary peroxisomal disorders (27, 28). Second, regarding BA metabolism, although levels of commonly used peroxisomal markers THCA and DHCA were undetectable, changes in C24-conjugated BAs (lower in LSFC patients and H-*Lrpprc*$^{-/-}$ mice) suggest a lower rate of conjugation of BAs (41, 42). Finally, changes in plasmalogen levels (lower in plasma of LSFC patients and H-*Lrpprc*$^{-/-}$ mice, higher in livers of H-*Lrpprc*$^{-/-}$ mice) point to alterations in their synthesis and/or secretion. The exact molecular mechanism underlying these changes, particularly the differential response of plasma versus liver in H-*Lrpprc*$^{-/-}$ mice, remains, however, to be further investigated. Nevertheless, it is known that in contrast to other tissues such as the heart and brain, the liver presents under normal conditions very low steady-state levels of plasmalogens. This is ascribed to their rapid export — as lipoproteins — into circulation for extrahepatic metabolism (35, 43). Therefore, possible explanations include a mismatch between their hepatic export via lipoproteins and extrahepatic uptake and/or enhanced hepatic synthesis as a compensatory mechanism to normalize their blood levels. The biosynthesis of plasmalogens is regulated by their intracellular levels through a negative feedback mechanism involving the enzyme FAR1 (33, 34, 44, 45). This plasmalogen-sensing mechanism occurs in the inner leaflet of the plasma membrane and the signal is subsequently transferred to peroxisomes (33). Our finding of a higher level of transcripts for *Far1* and of *Agps* in the liver of H-*Lrpprc*$^{-/-}$ mice would be consistent with its activation, which in turn would enhance their peroxisomal biosynthesis, and result in a higher concentration of plasmalogens when assessed in liver tissue homogenates.

LRPPRC-dependent mitochondrial dysfunction triggers broad changes in the lipidomic landscape reminiscent of NAFLD. One striking observation made in this study bears broader relevance beyond primary gene defects in mitochondria or peroxisomes. This pertains to plasma and hepatic lipid perturbations observed in H-*Lrpprc*$^{-/-}$ mice, which are reminiscent of those reported in humans with NAFLD as well as in animal models of the disease (31, 32, 46–48). These include (i) higher triglycerides, LCACs, and PE to PC ratio in the liver, and (ii) reduced levels of cholesteryl ester, plasmalogens, and DHA (free and bound to PCs), along with increased plasma levels of PCs containing a 22:5 FA (a precursor of DHA synthesis). Consistent with these observations, microvesicular steatosis and cholestasis, 2 key histopathological features of steatosis (49), have been reported in both H-*Lrpprc*$^{-/-}$ mice and LSFC patients (8, 15).

Linking mitochondrial dysfunction to peroxisomal metabolic disturbances: potential mechanisms and clinical implication. Taken together, the results from this study focusing on a monogenic mitochondrial disease, and from previous ones on primary peroxisomal defects (20, 21, 49), highlight the crucial reciprocal crosstalk between mitochondria and peroxisomes in order to maintain normal systemic and hepatic lipid metabolism. Figure 7 recapitulates the perturbations of mitochondrial and peroxisomal lipid metabolism observed in this study following LRPPRC-dependent mitochondrial dysfunction in humans and its transgenic mouse model. Further investigations will be needed to elucidate the molecular mechanisms linking the primary defect in mitochondrial function to secondary perturbations of peroxisomal lipid metabolism, particularly the impaired synthesis of DHA, as well as the conjugation of BAs. The changes in liver VLCACs (up in H-*Lrpprc*$^{-/-}$ mice) are, however, likely to result from an enhanced elongation of LCFAs to VLCFAs, which are substrates for peroxisomal β-oxidation (50), as well as from a mismatch between the formation of VLCFAs and their peroxisomal metabolism. The latter notion is reinforced by changes in transcript levels that were observed for *Acox1* (down) and *Ehhadh* (up), and/or peroxisomal biogenesis. Regarding plasmalogens, as mentioned earlier, it appears likely that their higher levels measured in livers of H-*Lrpprc*$^{-/-}$ mice reflect their enhanced peroxisomal synthesis following Far1 sensing of lower plasmalogens at the surface of the peroxisomal membrane, which in turn drives *Far1* gene expression.

Irrespective of the mechanisms involved, the observed perturbations in peroxisomal lipid metabolism, which are likely to be predominant in the liver, could also have a negative impact on other tissues, particularly the brain. Indeed, plasmalogens are highly enriched in polyunsaturated FAs (especially DHA), they account for approximately 20% of phospholipids in the adult brain (51), and they represent essential components of myelin (52). In human peroxisomal disorders (e.g., rhizomelic chondroplasia punctata and Zellweger spectrum) as well as in their mouse models, low levels of plasmalogens are associated with several

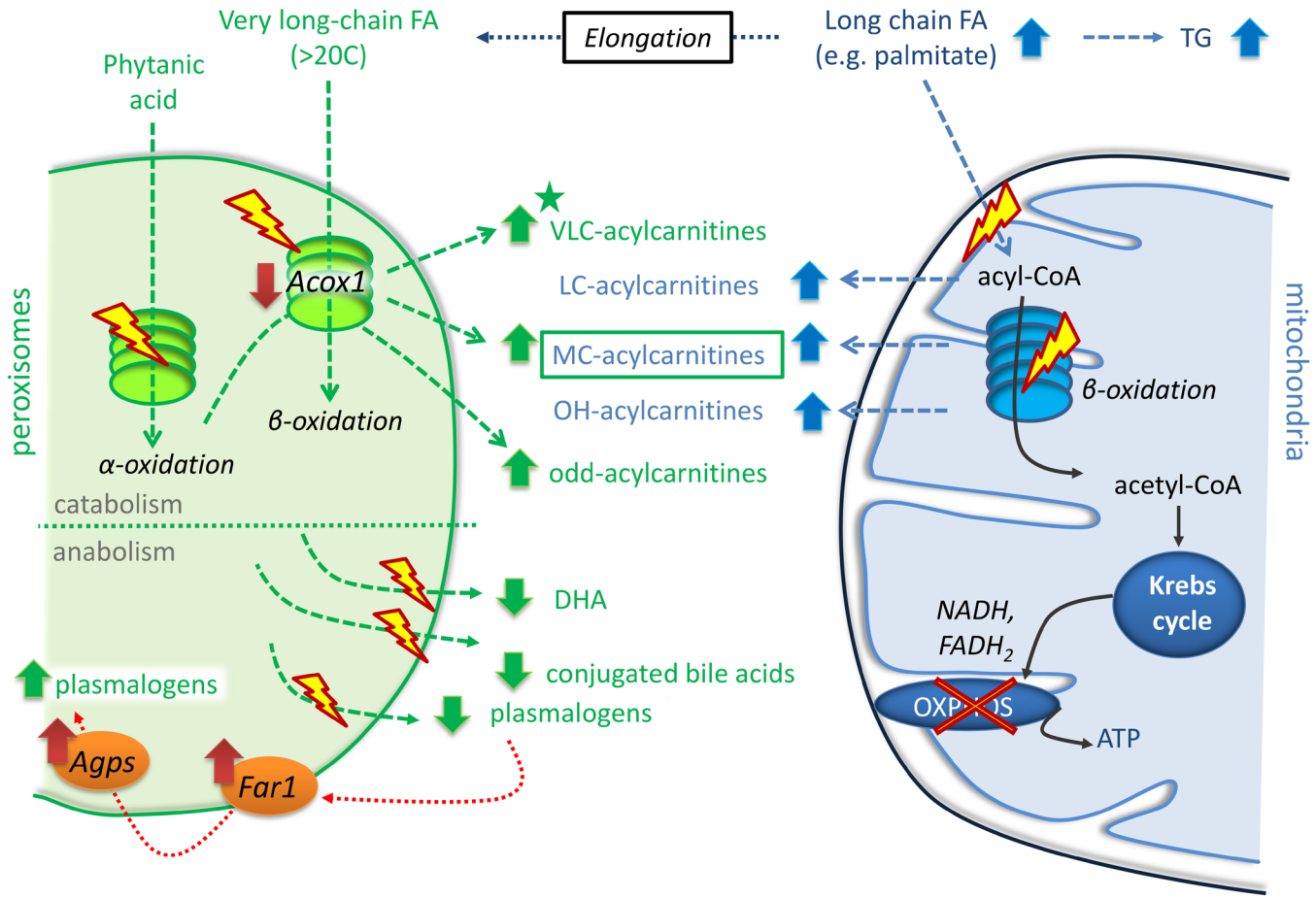

Figure 7. Mitochondrial and peroxisomal pathway contribution to the lipidomic signature observed in LSFC patients and in H-*Lrpprc*$^{-/-}$ mice. This schematic depicts the metabolic pathways in mitochondria (in blue) and peroxisomes (in green) that are related to the lipid perturbations reported in this study (increased or decreased levels, as indicated by upward or downward arrows, respectively) in plasma and/or liver (the green star indicates changes in liver only). The lightning bolt indicates the proposed sites of pathway perturbations. Beyond OXPHOS deficiency, LRPPRC-dependent mitochondrial dysfunction results in major perturbations of lipid metabolism. Here we confirm and extend our previous observations of an important dysregulation of mitochondrial FA β-oxidation (12, 15), as suggested by the accumulation of ACs of various chain length, especially LCACs, MCACs, and hydroxylated ACs. This dysregulation is likely to result in cytosolic FA overflow, which favors tissue triglyceride (TG) accumulation, but also FA elongation, which in turn promotes the synthesis of VLCFAs, which are substrates for peroxisomal β-oxidation (shown in green). The accumulation in VLCACs in liver tissues suggests, however, a mismatch between VLCFA formation and their peroxisomal oxidation, which may be reduced as suggested by decreased *Acox1* (downward red arrow) expression in liver. The presence of additional perturbations in peroxisomal metabolism is also reflected by changes in livers and plasma of (i) odd-numbered carbon chain ACs (increased), which may result from impaired phytanic acid oxidation, as well as (ii) lower levels of DHA and conjugated bile acids. Lastly, this is also reflected by the lower circulating levels of plasmalogens, which may exert a positive feedback (red dashed arrow) on *Far1* expression (upward red arrow), and thereby result in enhanced hepatic plasmalogen biosynthesis (suggested by higher *Agps* expression; upward red arrow) and tissue levels.

brain abnormalities such as hypomyelination, microglia neuroinflammation, defect in neuronal migration, and abnormal cerebellum formation (52–57). Consequently, our finding of low levels of circulating plasmalogens opens a potentially novel perspective on the molecular mechanisms underlying the neurological manifestations in LSFC, and possibly also for other forms of Leigh syndrome.

Using a comprehensive lipidomic approach in human and mouse carrying LRPPRC-dependent mitochondrial dysfunction, we unveil a major lipid dyshomeostasis, which beyond involving the mitochondrion, reflect also metabolic repercussions on other compartments, particularly the peroxisome. These perturbations encompass plasma and hepatic changes in plasmalogens, BA conjugates, as well as of VLC and odd-numbered carbon chain ACs, which are reminiscent of those reported in primary peroxisomal disorders, albeit more subtle, than those reported in primary peroxisomal disorders, as expected for changes secondary to a primary mitochondrial dysfunction. Of potential broader relevance, they also include other major lipid changes evocative of NAFLD; this is consistent with the previously reported microvesicular steatosis and cholestasis in H-*Lrpprc*$^{-/-}$ mice and LSFC patients (8, 16). Collectively, these findings highlight the crucial reciprocal

crosstalk between mitochondria and peroxisomes that takes place in order to maintain normal systemic and hepatic lipid metabolism. They also underscore the value of lipidomics as applied to both a human cohort and its study model to unveil complex and unexpected mechanisms underlying lipid dyshomeostasis ensuing from mitochondrial dysfunction. More studies will, however, be needed in order to further determine whether the identified lipid perturbations, particularly low plasma plasmalogens, may affect tissues other than the liver, such as the brain, and thereby account for some of the extrahepatic manifestations observed in patients with LSFC or other primary mitochondrial diseases, as well as in patients with acquired NAFLD.

Methods

Reagents

All solvents for MS analyses were purchased from Fisher Chemical, except for acetone and ethyl acetate, which were from JT Baker, ammonium formate from Sigma-Aldrich, and hydrochloric acid from Fisherbrand.

Experimental animals

The generation of liver-specific *Lrpprc*-null mice (H-*Lrpprc*$^{-/-}$) has been previously described in detail (15). Animals were housed in a specific pathogen–free facility under a 12-hour light/12-hour dark cycle at constant temperature and had free access to water and standard chow diet. At 14 weeks of age, animals (50% male, 50% female) were euthanized with chloral hydrate (8%, 6 g/kg) for liver excision and blood collection.

Human cohort

The cohort consisted of 8 LSFC patients that were homozygous for the A354V founder mutation and 1 additional patient, heterozygous for this mutation, with a premature stop codon (C1277STOP) in the *LRPPRC* gene. These patients were prospectively matched to 9 control subjects for gender, age (±2 years for children <18 years; ±5 years for adults >18 years), body mass index (BMI; ±10 percentiles of BMI for age for children; ±3 kg/m^2 for adults), and physical activity level (8 of 9 sedentary, including activities of daily living and walking less than 30 min/day; 1 of 9 moderately active, including activities of daily living and 30 to 60 min/day activity of moderate intensity). Carrying A354V and C1277STOP was an exclusion criterion for controls. Venous blood was collected after an overnight fast of minimum 12 hours, and 90 minutes after consuming a standardized smoothie (0.55 Kcal/mL) having the following composition for 100 mL: 5.7 g total carbohydrate, 0.7 g fiber, 4.0 g sugar, 1.6 g protein, 2.8 g total lipid, 0.2 g saturated fat, 1.6 g monounsaturated fat, 1.1 g polyunsaturated fat, 0.8 g n-6 fatty acids, 0.2 g n-3 fatty acids, 16 mg sodium, and 115 mg potassium.

Sample collection

Humans. Home visits along with a standardized sampling blood protocol were conducted in order to minimize the testing burden for the family and reduce variability related to environmental factors. Venous blood was collected in EDTA BD Vacutainer tubes, immediately placed on ice, and centrifuged within 30 minutes of collection at 2,000 *g* for 15 minutes. Plasma was immediately put on ice, aliquoted into Sarstedt microtubes, frozen on dry ice, and stored at –80°C until analysis. All analyses were performed on frozen aliquots that had not been previously thawed.

Animals. Blood was collected in EDTA BD Vacutainer tubes from the inferior vena cava and immediately put on ice for at least 30 minutes, prior to centrifugation at 2,000 *g* for 15 minutes at 4°C. Plasma samples were aliquoted and stored at –80°C. Prior to tissue harvesting, heart was perfused through the aorta with cold isotonic NaCl solution (0.9%, 10 mL) and livers were then quickly excised and snap-frozen (<5 seconds) in liquid nitrogen and stored at –80°C before further experimentations.

Sample processing and analysis by LC-MS

General procedure. Samples were processed for metabolite extraction and analysis by LC-MS following different protocols and methods, namely: (i) untargeted lipidomics using high-resolution LC-QTOF (Agilent 6530 and 6550 accurate-mass, Agilent Technologies Inc.), as well as targeted analyses using LC-QQQ (Agilent 6495 or 6460, Agilent Technologies Inc.) for (ii) plasmalogens, (iii) ACs, (iv) VLCACs and LPC, and (v) BAs. For plasma, a volume of 100 μL was used for all analyses prior to solubilization in the appropriate solvent. For targeted profiling of ACs or BAs, samples were homogenized (45 seconds, high intensity, Bead Ruptor homogenizer, Omni International) in the appropriate solvent (indicated below) supplemented with 3 ceramic

beads (2.8 mm). For tissue, freeze-clamped livers were ground at the temperature of liquid nitrogen. The resulting tissue powder was weighed (~50 mg, unless otherwise specified) and homogenized in the appropriate solvent (indicated below) supplemented with 6 ceramic beads (2.8 mm; 45 seconds, high intensity, Bead Ruptor homogenizer), except for ACs for which samples were sonicated (20 seconds, repeated twice, 4°C).

Untargeted lipidomic analyses using LC-QTOF. Untargeted lipidomic analyses were performed using a previously validated workflow (25), which is herein briefly summarized. Lipids were extracted from plasma or liver after spiking with the following internal standards: LPC 13:0, PC19:0/19:0, PC14:0/14:0, PS12:0/12:0, PG15:0/15:0, and PE17:0/17:0 (Avanti Polar Lipids Inc). Sample (0.7 μL for positive mode and 2 μL for negative mode) was injected into a 1290 Infinity HPLC coupled to a 6530 accurate mass QTOF MS system equipped with a dual electrospray ionization (ESI) source and analyzed in both positive and negative scan mode. A Zorbax Eclipse plus column (C18, 2.1 mm × 100 mm, particle size 1.8 μm, Agilent Technologies Inc.) was used for lipid elution over 83 minutes at constant temperature of 40°C using a gradient of solvent A (0.2% formic acid and 10 mM ammonium formate in water) and B (0.2% formic acid and 5 mM ammonium formate in methanol/acetonitrile/methyl *tert*-butyl ether [MTBE], 55:35:10 [v/v/v]). MS data processing was achieved using the Mass Hunter Qualitative Analysis software package (version B.06 for 6530-QTOF, and version B.07 for 6550-QTOF) and a bioinformatic script that we have developed and encoded in both Perl and R languages to enable optimal MS data alignment. This results in an updated and ready-to-use data set listing features with their mass, corrected signal intensity, and retention time. Lipid identification was achieved using MS/MS and the resulting files were aligned with previously acquired MS files prior to manual interpretation in silico similar to Godzien et al. (58). Briefly, identification of lipid structure, including FA side chains, was performed by (i) searching the *m/z* of selected features in METLIN or LIPID MAP databases, and (ii) identifying using the MS/MS spectra the polar head and acyl chains based on their signature fragment ion. For some ether lipids, it was difficult to distinguish plasmanyl (O-alkyl) from plasmenyl (P-alkyl) glycerophospholipids since MS/MS identifies the number of unsaturation on acyl chains, but not their position. Hence, ether lipids were annotated as "O-alkyl" and referred to as "plasmalogens." In some instances, identification of plasmalogens in a given data set was achieved by manual alignment with previously acquired human and mouse data sets for which the various plasmalogens had been identified by MS/MS.

Plasmalogen analysis on LC-QQQ. One aliquot of samples processed for untargeted lipidomic analysis was used for semiquantitative analysis of plasmalogens. This was assessed by dynamic multiple reaction monitoring (MRM) acquisition in negative ionization using a 6460 QQQ equipped with an electrospray standard source and coupled with a 1290 Infinity HPLC. Chromatographic conditions were identical to those described above for the untargeted lipidomic analysis using LC-QTOF. A volume of 2 μL (corresponding to 0.6 μL of plasma) was injected into the LC-QQQ. The collisional energy was optimized for each transition. MRM transitions are reported in Supplemental Table 4 and differed for the various plasmalogen (sub)classes: 2 transitions were measured for PC species, which included a fragment representative of the acyl chain sn2 (transition 1) and the loss of methyl formate (mass 60; transition 2), 1 for PE (transition 1) and LPC (transition 2). Data were processed using Mass Hunter Quantitative Analysis software (version B.06). MS signal intensity data for all plasmalogens are reported as ratios relative to the MS signal intensity of the internal standard PC 14:0/14:0.

Global AC analysis using LC-QQQ. Profiling of 91 ACs was performed using a previously described semiquantitative method (24, 59) with slight modifications. Briefly, plasma samples or pulverized liver tissues previously freeze-clamped were homogenized in acetonitrile and spiked with deuterated standards prepared in methanol or 50% methanol/50% H_2O ([$^2H_9$]carnitine, [$^2H_3$]octanoylcarnitine, and [U-^{13}C]palmitoylcarnitine from Sigma-Aldrich; and [$^2H_3$]acetylcarnitine, [$^2H_3$]propionylcarnitine, [$^2H_3$]butyrylcarnitine, and [$^2H_3$]dodecanoyl from CDN Isotopes) before freezing at –20°C for 20 minutes. After centrifugation (7,500 *g*, 10 minutes), the supernatants were combined and evaporated to dryness under a stream of nitrogen gas before suspension with 50 μL of methanol and 50 μL of H_2O. Subsequently, 2 μL was injected into a 1290 Infinity HPLC equipped with an Atlantis dC18 silica column (50 mm × 4.6 mm, particle size 3 μm; Waters) coupled to a 6460 QQQ MS/MS system by an ESI Jet Stream source. Chromatographic separation was achieved using a gradient of solvent A (100% water/0.2% formic acid/10 mM ammonium formate) and solvent B (95% acetone/5% MTBE/0.2% formic acid) as follows: (i) 100% solvent A for 4.5 minutes, (ii) a linear gradient of solvent B that reached 50% at 33 minutes and (iii) then increased to 100% from 33 minutes to 54 minutes, and (iv) 100% solvent A for 5 minutes to re-equilibrate the column. The flow rate

was maintained at 0.5 mL/min throughout the run time. Data were monitored in positive ionization and dynamic MRM mode for product ions *m/z* 85 and *m/z* 60 on which the last one was used as qualifier, as previously reported (24, 54). Data were processed by Mass Hunter QQQ Quantitative Analysis software (version B.07). MS signal intensity data for all ACs are reported as ratios relative to the MS signal intensity of their corresponding internal standard (the closest in terms of chain length). This method enables a global analysis of ACs, albeit it was found not to be ideally suited for VLCAC analysis. Hence, we developed a specific semiquantitative method for VLCACs, which also includes LPC 26:0, given the reported correlation between AC26:0 and LPC 26:0 in peroxisomal disorders (27, 28).

VLCAC and LPC 26:0 analysis using LC-QQQ. The procedure for sample preparation was essentially that described for our untargeted lipidomics (25) with slight modifications. Briefly, plasma (100 μL) or liver (40 mg) was spiked with the following internal labeled standards: [$^2H_9$]hexacosanoylcarnitine and [U-^{13}C]26:0-lysophosphatidylcholine (Millipore Sigma). Samples were injected (4 and 3 μL respectively for plasma and liver) into a 1290 Infinity HPLC equipped with an Hypersil GOLD column (C8, 150 × 2.1 mm, particle size 3 μm; Thermo Fisher Scientific). Chromatographic separation was achieved using a gradient of solvent A (100% water/5 mM ammonium formate/5 mM ammonium acetate) and solvent B (55% methanol/35% acetonitrile/10% MTBE/5 mM ammonium formate/0.2% formic acid) as follows: (i) 100% solvent A for 4.5 minutes; (ii) a linear gradient of solvent B that reached 99.5% at 30 minutes, which was maintained from 30 minutes to 50 minutes; and (iv) 100% solvent A for 5 minutes to re-equilibrate the column. The flow rate was maintained at 0.2 mL/min throughout the run time. MS analyses were performed with a 6495 QQQ equipped with an AJS ESI source operating in positive mode. Analytes were monitored by MRM; mass transitions, collision energy and CV are reported in Supplemental Table 5. Blanks were inserted after 4 runs to prevent carryover. MS signal intensity data for VLCACs and LPC 26:0 are reported as ratios relative to the MS signal intensity of internal standard.

BA analysis using LC-QQQ. Procedures for BA extraction and semiquantitative analysis were based on previously described methods with slight modifications (60, 61). Briefly, plasma samples or pulverized liver tissues previously freeze-clamped (20 mg) were homogenized in methanol/water (80:20, v/v) spiked with deuterated standards ([$^2H_4$]lithocholic acid, d_4-LCA; [$^2H_4$]cholic acid, d_4-CA; [$^2H_4$]chenodeoxycholic acid, d_4-CDCA; [$^2H_4$]deoxycholic-2,2,4,4-d_4 acid, d_4-DCA); [$^2H_4$]glycodeoxycholic acid, d_4-GDCA; [$^2H_4$]glycochenodeoxycholic acid, d_4-GCDCA; and [$^2H_4$]glycocholic acid, d_4-GCA) (CDN Isotopes) and then acidified with HCl (1 mM) before homogenization and centrifugation. The supernatants were extracted again with methanol/water (80:20, v/v). After centrifugation, the newly collected supernatant was concentrated to a final volume of 100 μL under a stream of nitrogen before sonication and transfer to glass vials as three aliquots for storage at –80°C. For LC-MS analysis, 10 μL (plasma) or 4 μL (liver) was injected into a 1290 Infinity HPLC equipped with a Synergi Fusion-RP column set at 40°C (polar embedded C18, 100 mm × 2 mm, particle size 2.5 μm; Phenomenex) coupled to a 6495 QQQ mass spectrometer by a Jet Stream Electrospray source. Chromatographic separation was achieved using a gradient of solvent A (100% water/10 mM ammonium formate/0.02% formic acid) and solvent B (55% methanol/35% acetonitrile/10% MTBE/0.02% formic acid) as follows: (i) 100% solvent A for 6 minutes, (ii) a linear gradient of solvent B that reached 100% at 50 minutes and (iii) maintained from 50 to 67 minutes, and (iv) 100% solvent A for 10 minutes to re-equilibrate the column. The flow rate was set at 0.4 mL/min until 60.5 minutes and increased at 0.5 mL/min from 60.5 to 67.5 minutes. Data were monitored in negative ion and MRM mode and processed by Mass Hunter QQQ Quantitative Analysis software (version B.07). MS signal intensity data for all measured BAs are reported as ratios relative to the MS signal intensity of their corresponding internal standard. Supplemental Table 6 lists all BAs and their respective internal standards, along with their MRM mass transition. Supplemental Table 7 reports intraday (5 independent sample preparations) as well as interday (3 independent days) coefficient of variation values for the entire workflow for each BA spiked in plasma samples as well as their LC-MS signal reproducibility (3 independent injections of the same sample).

Quantitative LC-MS analysis of specific markers of peroxisomal disorders. Plasma samples from LSFC patients were sent to a diagnostic laboratory specialized in peroxisomal disorders (Laboratory Genetic Metabolic Diseases, Amsterdam, The Netherland; https://www.amc.nl/web/laboratory-genetic-metabolic-diseases-lgmd.htm) for the combined analysis of LPC 26:0 and AC26:0, as previously described (27) as well as of BA intermediates, particularly the precursors di- and trihydroxycholestanoic acid (DHCA and THCA), which were measured according to a previous study (62).

Molecular analyses

Quantitative RT-PCR. Gene transcript levels from frozen liver tissue were assessed as previously described for heart (59) using an RNeasy kit (QIAGEN) and reverse transcribed with the High-Capacity cDNA RT kit (Thermo Fisher Scientific) according to the manufacturer's recommendations. Quantification was achieved by MxPro software (Agilent Technologies Inc.) and reported using the standard curve method, then validated with the ΔΔCT method; the efficiency of the quantitative PCR reaction was set acceptable at 100% ± 10%. Gene transcript levels were normalized to the polymerase (RNA) II (DNA directed) polypeptide A (*Polr2a*) gene, selected among 7 housekeeping genes (list in Supplemental Table 8) for its stable relative quantity in H-*Lrpprc*$^{-/-}$ mice compared to their littermates. The list of primers used is reported in Supplemental Table 7.

Immunoblot. Protein levels from frozen liver tissue were assessed as previously described for heart (59). Primary antibodies against LRPPRC (1:10,000; catalog PA5-22034) and pan-cadherin (1:10,000; catalog 71-7100) were purchased from Thermo Fisher Scientific, catalase (1:50,000; catalog ab16731) and OXPHOS (1:2,000; catalog ab110413) from Abcam, and secondary antibodies, HRP-conjugated anti-rabbit (catalog 7074) or anti–mouse IgG (catalog 7076), were purchased from Cell Signaling Technology. Except for OXPHOS, for which pan-cadherin served as loading control, an HRP-conjugated β-actin–specific antibody (1:30,000; catalog sc-47778) was used to visualize β-actin for normalization (Santa Cruz Biotechnology).

Statistics

For lipidomic analysis, the output text file containing the processed data was imported into Mass Professional Pro (MPP: version 12.6.1; Agilent Technologies Inc.) for statistical analyses. Independent testing of each feature was achieved using paired (human) or 2-tailed unpaired (animals) Student's *t* test with Benjamini-Hochberg correction. We applied a threshold of corrected *P* values (*P-corr*) as an estimation of false discovery rate (FDR) of 20% (human) and 5% (animals) (untargeted lipidomics) and we report *P* values before and after Benjamini-Hochberg correction. For the molecular analyses, data were tested for significance using paired (patients) or 2-tailed unpaired (animals) Student's *t* test (GraphPad Prism software; version 5) and a threshold of *P* value of <0.05 was considered to be statistically significant. Data are depicted as volcano plots, dot plots, or box plots, where the midline represents the median; the box represents the interquartile range (IQR) between the first and third quartile, and whiskers represent the lowest or highest values.

Study approval and subject details

Humans. Studies followed protocols approved by the Human Ethics and Research Committee of the Centre de Santé et de Services Sociaux de Chicoutimi (Chicoutimi, Quebec, Canada). Written informed consent was obtained for all study participants or their legal guardians, when applicable. All human subjects were recruited between September 2011 and April 2012, as previously published (12).

Animals. Studies were approved by the Animal Research Ethics Committee of Université de Montréal in agreement with the guidelines of the Canadian Council on Animal Care.

Author contributions

MR and CDR contributed to the design of the study. MR performed most of the experiments with AF, CD, IRF, and BB for the lipidomic analyses. SD performed molecular experiments during the revision process. FMV was responsible for the analysis of markers of peroxisomal disorders. MR analyzed all the results. AC and YB provided samples from the mouse model essential for the study. JTL was directly involved in patient recruitment and supervised the research protocol. MR, CDR, and YB wrote, reviewed, and edited the manuscript. JDR reviewed and edited the manuscript. The LSFC Consortium provided biological samples. All authors commented on the results and the manuscript.

Acknowledgments

The authors thank Pascaline Morue and Frédérique Dupuis for their assistance with molecular analyses, Gabrielle Boucher with statistical analyses, Luc Vachon for helpful discussions, R.J. Wanders for his assistance in contacting the Diagnostic Laboratory in The Netherlands, and Antoinette Paolitto for secretarial assistance. We also gratefully acknowledge LSFC patients, their families, and the AAL (http:/www.aal.qc.ca). See Supplemental Acknowledgments for Consortium details. This work was supported by the Canadian Institutes of Health Research (CIHR) grants 9575 (awarded to CDR) and 102168 (awarded to CDR, JDR, and YB); Association de l'acidose lactique (AAL); Fondation du Grand Défi Pierre Lavoie; as well as the

Montreal Heart Institute Foundation and benefited from infrastructure supported by the Canadian Foundation for Innovation. JDR holds the Canada Research Chair in Genetics and Genomic Medicine. The funders had no role in study design, data collection and analysis, decision to publish, or preparation of the manuscript.

Address correspondence to: Yan Burelle, Faculty Health Sciences, University of Ottawa, RGN Building, 451 Smyth Road, Ottawa, Ontario K1N 8M5, Canada. Phone: 613.562.8000 ext. 8130; Email: yburell2@uottawa.ca. Or to: Christine Des Rosiers, Montreal Heart Institute Research Centre, 5000 Belanger Street, Montreal, Quebec H1T1C8, Canada. Phone: 514.376.3330 ext. 3594; Email: christine.des.rosiers@umontreal.ca.

1. Debray FG, Lambert M, Mitchell GA. Disorders of mitochondrial function. *Curr Opin Pediatr*. 2008;20(4):471–482.
2. Lightowlers RN, Taylor RW, Turnbull DM. Mutations causing mitochondrial disease: What is new and what challenges remain? *Science*. 2015;349(6255):1494–1499.
3. Lightowlers RN, Chrzanowska-Lightowlers ZM. Human pentatricopeptide proteins: only a few and what do they do? *RNA Biol*. 2013;10(9):1433–1438.
4. Manna S. An overview of pentatricopeptide repeat proteins and their applications. *Biochimie*. 2015;113:93–99.
5. Mootha VK, et al. Identification of a gene causing human cytochrome c oxidase deficiency by integrative genomics. *Proc Natl Acad Sci USA*. 2003;100(2):605–610.
6. Oláhová M, et al. LRPPRC mutations cause early-onset multisystem mitochondrial disease outside of the French-Canadian population. *Brain*. 2015;138(Pt 12):3503–3519.
7. Han VX, Tan TS, Wang FS, Tay SK. Novel LRPPRC mutation in a boy with mild leigh syndrome, French-Canadian type outside of Québec. *Child Neurol Open*. 2017;4:2329048X17737638.
8. Morin C, et al. Clinical, metabolic, and genetic aspects of cytochrome C oxidase deficiency in Saguenay-Lac-Saint-Jean. *Am J Hum Genet*. 1993;53(2):488–496.
9. Debray FG, et al. LRPPRC mutations cause a phenotypically distinct form of Leigh syndrome with cytochrome c oxidase deficiency. *J Med Genet*. 2011;48(3):183–189.
10. Sasarman F, Brunel-Guitton C, Antonicka H, Wai T, Shoubridge EA, LSFC Consortium. LRPPRC and SLIRP interact in a ribonucleoprotein complex that regulates posttranscriptional gene expression in mitochondria. *Mol Biol Cell*. 2010;21(8):1315–1323.
11. Sasarman F, Nishimura T, Antonicka H, Weraarpachai W, Shoubridge EA, LSFC Consortium. Tissue-specific responses to the LRPPRC founder mutation in French Canadian Leigh syndrome. *Hum Mol Genet*. 2015;24(2):480–491.
12. Thompson Legault J, et al. A metabolic signature of mitochondrial dysfunction revealed through a monogenic form of Leigh syndrome. *Cell Rep*. 2015;13(5):981–989.
13. Liu L, et al. LRP130 protein remodels mitochondria and stimulates fatty acid oxidation. *J Biol Chem*. 2011;286(48):41253–41264.
14. Lei S, et al. Increased hepatic fatty acids uptake and oxidation by LRPPRC-driven oxidative phosphorylation reduces blood lipid levels. *Front Physiol*. 2016;7:270.
15. Cuillerier A, et al. Loss of hepatic LRPPRC alters mitochondrial bioenergetics, regulation of permeability transition and trans-membrane ROS diffusion. *Hum Mol Genet*. 2017;26(16):3186–3201.
16. Akie TE, Liu L, Nam M, Lei S, Cooper MP. OXPHOS-mediated induction of NAD+ promotes complete oxidation of fatty acids and interdicts non-alcoholic fatty liver disease. *PLoS ONE*. 2015;10(5):e0125617.
17. Simões ICM, Fontes A, Pinton P, Zischka H, Wieckowski MR. Mitochondria in non-alcoholic fatty liver disease. *Int J Biochem Cell Biol*. 2018;95:93–99.
18. Baes M, Van Veldhoven PP. Hepatic dysfunction in peroxisomal disorders. *Biochim Biophys Acta*. 2016;1863(5):956–970.
19. Wanders RJ, Waterham HR, Ferdinandusse S. Metabolic interplay between peroxisomes and other subcellular organelles including mitochondria and the endoplasmic reticulum. *Front Cell Dev Biol*. 2015;3:83.
20. Peeters A, et al. Mitochondria in peroxisome-deficient hepatocytes exhibit impaired respiration, depleted DNA, and PGC-1α independent proliferation. *Biochim Biophys Acta*. 2015;1853(2):285–298.
21. Dirkx R, et al. Absence of peroxisomes in mouse hepatocytes causes mitochondrial and ER abnormalities. *Hepatology*. 2005;41(4):868–878.
22. Cherkaoui-Malki M, Surapureddi S, El-Hajj HI, Vamecq J, Andreoletti P. Hepatic steatosis and peroxisomal fatty acid beta-oxidation. *Curr Drug Metab*. 2012;13(10):1412–1421.
23. Violante S, et al. Peroxisomes contribute to the acylcarnitine production when the carnitine shuttle is deficient. *Biochim Biophys Acta*. 2013;1831(9):1467–1474.
24. Ruiz M, et al. Circulating acylcarnitine profile in human heart failure: a surrogate of fatty acid metabolic dysregulation in mitochondria and beyond. *Am J Physiol Heart Circ Physiol*. 2017;313(4):H768–H781.
25. Forest A, et al. Comprehensive and reproducible untargeted lipidomic workflow using LC-QTOF validated for human plasma analysis. *J Proteome Res*. 2018;17(11):3657–3670.
26. Lodhi IJ, Semenkovich CF. Peroxisomes: a nexus for lipid metabolism and cellular signaling. *Cell Metab*. 2014;19(3):380–392.
27. Klouwer FCC, et al. Evaluation of C26:0-lysophosphatidylcholine and C26:0-carnitine as diagnostic markers for Zellweger spectrum disorders. *J Inherit Metab Dis*. 2017;40(6):875–881.
28. Huffnagel IC, et al. Comparison of C26:0-carnitine and C26:0-lysophosphatidylcholine as diagnostic markers in dried blood spots from newborns and patients with adrenoleukodystrophy. *Mol Genet Metab*. 2017;122(4):209–215.
29. Wanders RJ, Ferdinandusse S. Peroxisomes, peroxisomal diseases, and the hepatotoxicity induced by peroxisomal metabolites. *Curr Drug Metab*. 2012;13(10):1401–1411.
30. Diaz F, et al. Pathophysiology and fate of hepatocytes in a mouse model of mitochondrial hepatopathies. *Gut*. 2008;57(2):232–242.
31. Gorden DL, et al. Biomarkers of NAFLD progression: a lipidomics approach to an epidemic. *J Lipid Res*. 2015;56(3):722–736.

32. Arendt BM, et al. Nonalcoholic fatty liver disease is associated with lower hepatic and erythrocyte ratios of phosphatidylcholine to phosphatidylethanolamine. *Appl Physiol Nutr Metab*. 2013;38(3):334–340.
33. Honsho M, Abe Y, Fujiki Y. Plasmalogen biosynthesis is spatiotemporally regulated by sensing plasmalogens in the inner leaflet of plasma membranes. *Sci Rep*. 2017;7:43936.
34. Honsho M, Asaoku S, Fujiki Y. Posttranslational regulation of fatty acyl-CoA reductase 1, Far1, controls ether glycerophospholipid synthesis. *J Biol Chem*. 2010;285(12):8537–8542.
35. Braverman NE, Moser AB. Functions of plasmalogen lipids in health and disease. *Biochim Biophys Acta*. 2012;1822(9):1442–1452.
36. Lefort B, et al. Pharmacological inhibition of carnitine palmitoyltransferase 1 restores mitochondrial oxidative phosphorylation in human trifunctional protein deficient fibroblasts. *Biochim Biophys Acta Mol Basis Dis*. 2017;1863(6):1292–1299.
37. Holden HM, Banaszak LJ. L-3-hydroxyacyl coenzyme A dehydrogenase. The location of NAD binding sites and the bilobal subunit structure. *J Biol Chem*. 1983;258(4):2383–2389.
38. Corkey BE, Shirihai O. Metabolic master regulators: sharing information among multiple systems. *Trends Endocrinol Metab*. 2012;23(12):594–601.
39. van de Beek MC, et al. C26:0-carnitine is a new biomarker for X-linked adrenoleukodystrophy in mice and man. *PLoS ONE*. 2016;11(4):e0154597.
40. Fan CY, et al. Hepatocellular and hepatic peroxisomal alterations in mice with a disrupted peroxisomal fatty acyl-coenzyme A oxidase gene. *J Biol Chem*. 1996;271(40):24698–24710.
41. Savolainen K, et al. A mouse model for alpha-methylacyl-CoA racemase deficiency: adjustment of bile acid synthesis and intolerance to dietary methyl-branched lipids. *Hum Mol Genet*. 2004;13(9):955–965.
42. Ferdinandusse S, et al. A novel bile acid biosynthesis defect due to a deficiency of peroxisomal ABCD3. *Hum Mol Genet*. 2015;24(2):361–370.
43. Vance JE. Lipoproteins secreted by cultured rat hepatocytes contain the antioxidant 1-alk-1-enyl-2-acylglycerophosphoethanolamine. *Biochim Biophys Acta*. 1990;1045(2):128–134.
44. Honsho M, Asaoku S, Fukumoto K, Fujiki Y. Topogenesis and homeostasis of fatty acyl-CoA reductase 1. *J Biol Chem*. 2013;288(48):34588–34598.
45. Honsho M, Fujiki Y. Plasmalogen homeostasis - regulation of plasmalogen biosynthesis and its physiological consequence in mammals. *FEBS Lett*. 2017;591(18):2720–2729.
46. Puri P, et al. A lipidomic analysis of nonalcoholic fatty liver disease. *Hepatology*. 2007;46(4):1081–1090.
47. Ma DW, et al. Plasma phospholipids and fatty acid composition differ between liver biopsy-proven nonalcoholic fatty liver disease and healthy subjects. *Nutr Diabetes*. 2016;6(7):e220.
48. Chiappini F, Desterke C, Bertrand-Michel J, Guettier C, Le Naour F. Hepatic and serum lipid signatures specific to nonalcoholic steatohepatitis in murine models. *Sci Rep*. 2016;6:31587.
49. Baumgart E, et al. Mitochondrial alterations caused by defective peroxisomal biogenesis in a mouse model for Zellweger syndrome (PEX5 knockout mouse). *Am J Pathol*. 2001;159(4):1477–1494.
50. Tucci S, Behringer S, Spiekerkoetter U. De novo fatty acid biosynthesis and elongation in very long-chain acyl-CoA dehydrogenase-deficient mice supplemented with odd or even medium-chain fatty acids. *FEBS J*. 2015;282(21):4242–4253.
51. Dean JM, Lodhi IJ. Structural and functional roles of ether lipids. *Protein Cell*. 2018;9(2):196–206.
52. Berger J, Dorninger F, Forss-Petter S, Kunze M. Peroxisomes in brain development and function. *Biochim Biophys Acta*. 2016;1863(5):934–955.
53. Teigler A, Komljenovic D, Draguhn A, Gorgas K, Just WW. Defects in myelination, paranode organization and Purkinje cell innervation in the ether lipid-deficient mouse cerebellum. *Hum Mol Genet*. 2009;18(11):1897–1908.
54. Katafuchi T, et al. Effects of plasmalogens on systemic lipopolysaccharide-induced glial activation and β-amyloid accumulation in adult mice. *Ann N Y Acad Sci*. 2012;1262:85–92.
55. Hossain MS, et al. Reduction of ether-type glycerophospholipids, plasmalogens, by NF-κB signal leading to microglial activation. *J Neurosci*. 2017;37(15):4074–4092.
56. Müller CC, et al. PEX13 deficiency in mouse brain as a model of Zellweger syndrome: abnormal cerebellum formation, reactive gliosis and oxidative stress. *Dis Model Mech*. 2011;4(1):104–119.
57. Janssen A, et al. Neuronal migration depends on intact peroxisomal function in brain and in extraneuronal tissues. *J Neurosci*. 2003;23(30):9732–9741.
58. Godzien J, Ciborowski M, Martínez-Alcázar MP, Samczuk P, Kretowski A, Barbas C. Rapid and reliable identification of phospholipids for untargeted metabolomics with LC-ESI-QTOF-MS/MS. *J Proteome Res*. 2015;14(8):3204–3216.
59. Ruiz M, et al. MK2 deletion in mice prevents diabetes-induced perturbations in lipid metabolism and cardiac dysfunction. *Diabetes*. 2016;65(2):381–392.
60. Scherer M, Gnewuch C, Schmitz G, Liebisch G. Rapid quantification of bile acids and their conjugates in serum by liquid chromatography-tandem mass spectrometry. *J Chromatogr B Analyt Technol Biomed Life Sci*. 2009;877(30):3920–3925.
61. Tagliacozzi D, et al. Quantitative analysis of bile acids in human plasma by liquid chromatography-electrospray tandem mass spectrometry: a simple and rapid one-step method. *Clin Chem Lab Med*. 2003;41(12):1633–1641.
62. Bootsma AH, et al. Rapid analysis of conjugated bile acids in plasma using electrospray tandem mass spectrometry: application for selective screening of peroxisomal disorders. *J Inherit Metab Dis*. 1999;22(3):307–310.